DOI:10.1103/PhysRevD.51.4763
FERMILAB-PUB-94-453
MSU-HEP-41024
CTEQ-404

October, 1994

Global QCD Analysis and the CTEQ Parton Distributions[†]

H.L. Lai[a], J. Botts[a,b], J. Huston[a], J.G. Morfin[c], J.F. Owens[d], J.W. Qiu[e], W.K. Tung[a] and H. Weerts[a]

[a]Michigan State University, [b]DESY-Zeuthen,
[c]Fermi National Accelerator Laboratory,
[d]Florida State University, [e]Iowa State University

Abstract

The CTEQ program for the determination of parton distributions through a global QCD analysis of data for various hard scattering processes is fully described. A new set of distributions, CTEQ3, incorporating several new types of data is reported and compared to the two previous sets of CTEQ distributions. Comparison with current data is discussed in some detail. The remaining uncertainties in the parton distributions and methods to further reduce them are assessed. Comparisons with the results of other global analyses are also presented.

[†]This work is supported in part by DOE, NSF and TNRLC

1 Introduction

Calculations of high energy hard scattering processes in perturbative quantum chromodynamics (pQCD) rely on two basic ingredients – (1) the perturbatively calculated scattering cross-sections involving the fundamental partons, leptons, and gauge bosons and (2) the parton distributions inside the incoming hadrons. Our knowledge of these universal parton distributions functions (PDF's) is derived, in turn, from the analysis of data for a variety of hard scattering processes. Early analyses were often limited to deep inelastic lepton nucleon scattering and lepton pair production, as these were the processes for which extensive data sets were available and for which next-to-leading-order (NLO) calculations of the hard scattering subprocesses had been performed. Now the number of available NLO calculations has increased and, simultaneously, data for additional hard scattering processes have become available for a variety of beams and targets. This progress makes it possible to determine the parton distributions with a greater precision than was previously possible. Indeed, assumptions such as an SU(3) or SU(2) symmetry for the quark-antiquark sea in the proton have had to be discarded in the face of experimental evidence to the contrary.

With this wealth of data and corresponding theoretical calculations, true "global analyses" have become possible. In such a program there are two main goals. The first is to determine the parton distributions as precisely as possible, using all available experimental input, and to suggest which new types of data are necessary in order to further improve the precision. A review of progress in this area and references to earlier work can be found in Ref.[1]. Secondly, with an over-constrained set of PDF's it becomes possible to explore whether or not the parton-level calculations in pQCD constitute a consistent theoretical framework to account for all the available experimental data relevant for pQCD studies. This may point to areas where improved theoretical treatments are required and, perhaps, uncover areas where various data sets used in the analysis might be mutually inconsistent. Either way, one can expect important progress to be made as the result of careful and critical confrontation of data with theory. This potential has been discussed in some length in Ref.[2].

This paper describes the series of global analyses conducted by the CTEQ Collaboration.[1] The necessary tools for carrying out this systematic global analysis program have been developed from those used in the previous work of Duke, Owens, and collaborators [3], [4] and Morfin-Tung [5]. The use of two independent QCD parton evolution and global fitting programs provides a valuable consistency check on all aspects of the analysis. The CTEQ program is designed to systematically refine the PDF's as new theoretical and experimental advances are made, and to clearly describe the theoretical and experimental inputs and their relation to the resulting parton distributions. The different versions of CTEQ distributions reflect historically a series of different assumptions and inputs. As a general rule, newer versions incorporate more up-to-date data and are preferred *overall* than earlier ones, although this may not be an absolute statement because the multi-faceted nature of global analysis does not always lead to a one-dimensional progression of improvements—as will be-

[1]The CTEQ collaboration (Coordinated Theoretical/Experimental Project on QCD Phenomenology and Tests of the Standard Model) consists of, in addition to the above authors (as members of its global fit subgroup), S. Kuhlmann (ANL); S. Mishra (Harvard); R. Brock, J. Pumplin, C.P. Yuan (MSU); D. Soper (Oregon); J. Collins, J. Whitmore (PSU); F. Olness (SMU); and J. Smith, G. Sterman (Stony Brook).

come clear when these developments are described. It should be recognized that, in general, differences between current and prior PDF's are not a reflection of "theoretical uncertainties", but rather are indications of the manner in which new developments in data/theory impact on the determination the underlying parton distributions.

The first stage of this analysis (known as "CTEQ1"[6]), was performed in 1992 following the availability of the high precision deep inelastic scattering (DIS) data by the CCFR [7] and NMC [8] collaborations. A second, unpublished set (known as "CTEQ2"), spurred by new data from HERA [9], has been circulated during the past year.[2] The advent of recent data on the lepton asymmetry in $W-$boson production [10] and on the difference in Drell-Yan cross-sections from proton and neutron targets [11] has stimulated further refinements which result in a new set which will be referred to as "CTEQ3." The common features as well as differences amongst these three sets will be discussed in detail in this paper.

In Secs. 2 and 3 below, we review the various physical processes and experimental inputs included in our analysis and present a relatively self-contained account of the analysis and fitting procedures used. The development of the three versions of CTEQ distributions is described in Sec. 4, reserving the most detailed discussion to the latest version. Comparisons with other parton distributions and with recent data are described in Sec. 5. Some remaining uncertainties in the parton distributions and outstanding challenges are discussed in Sec. 6. Our conclusions are given in Sec. 7. Readers with immediate interest in results and recent developments can skip to Sec. 4 and refer back for necessary details.

A similar program of global analyses and continual upgrading of PDF's has been undertaken by the MRS group [12, 13]. The recently released MRS(H) distributions have now been revised and replaced by the MRS(A) set as a result of new data mentioned above.[3] A comparison of these results with those of our analysis is included in Sec.5.

2 Experimental Input

In order to make the comparison of theory with experiment well-defined, we have limited the kinematic range to that where the "leading twist" QCD contributions are dominant. Thus, we restrict the selection of experimental data to kinematic regions which contain at least one large momentum scale "Q" $> Q_{min}$. In the absence of a reliable theoretical guide in the perturbative formalism, the value Q_{min} is varied within the range $2-10$ GeV to test for sensitivity of the results to this choice. We found stable results generally with the following minimum kinematic constraints: for deep inelastic scattering, Q (virtuality of the vector boson) > 2 GeV and W (CM energy) > 3.5 GeV; for lepton-pair production, $Q > 4$ GeV; for direct photon production $p_T > 4$ GeV.

Recent high statistics DIS data from NMC [8] on $F_2^n/F_2^p, F_2^p - F_2^n$, and $F_2^{p,d}$ using a muon beam and from CCFR [7] on $F_{2,3}^{Fe}$ using (anti-) neutrinos, combined with the existing BCDMS [15] results provide excellent coverage of the kinematic region $x > 0.01$. New

[2] A brief description of these distributions has been given in Ref.[2].

[3] It is worth noting that the MRS analyses are based on the evolution and fitting package developed jointly by Duke, Owens, and Roberts some time ago [3], [4], [14]; hence the tools of analysis of the MRS and CTEQ groups, in fact, overlap. There are, however, differences in analysis procedures, data selection, and the handling of experimental errors.

measurements of F_2^p from HERA [9] have extended the kinematic range down to very small x values, approaching 10^{-4}. Although the errors are comparatively large, the extended range provides useful constraints on the behavior of the parton distributions in the small-x region. (Throughout this paper, "small-x" means $10^{-4} < x < 10^{-2}$.) As will be discussed in some detail in Sec. 4, this is particularly important in light of questions raised concerning the consistency of the structure functions measured in the other experiments in the intermediate region $0.01 < x < 0.1$ [6].

Precision data from the SLAC-MIT series of experiments [16] largely lie outside the kinematic cuts (especially when the cuts are raised above the minimum quoted above); and those data points within the cuts agree well with the BCDMS and NMC data already included. They are thus not used in the analyses reported here. Data from the earlier EMC experiment [17] are excluded since the disagreement between these data with other data sets appears to be understood now as the result of the new NMC analysis. Data from the CDHSW neutrino experiment [18] are also not used since in the (wide) region where they agree with the CCFR results, the latter completely dominate due to the much smaller errors; and in the (narrow) region where they disagree, it would be inconsistent to include both sets.[4]

To apply the selected experimental results to the study of the parton structure of the nucleon, the heavy target neutrino data must be converted to their nucleon equivalent. This conversion is done using measured light to heavy target ratios obtained in electron and muon scattering processes by the SLAC-MIT [19], EMC [20], and NMC [21] experiments. There is an uncertainty associated with this procedure, which will be commented on later.

DIS data by themselves are not sufficient to provide a complete set of constraints on the parton content of the nucleon, since the measured nucleon structure functions represent only a few independent combinations of the parton flavors. Lepton-pair production experiments provide a useful handle on the anti-quark distributions (through the $q - \bar{q}$ annihilation mechanism) and the gluon distribution (through the $q-g$ "Compton scattering" mechanism). From fixed-target experiments we use the full data set on the double-differential cross-section $d^2\sigma/d\tau dy$ measured by the high statistics E605 experiment at Fermilab [22]. We also include the new collider data on lepton-pairs measured by the CDF Collaboration [23]. Although the errors on these data are comparatively large, they do provide some constraints in the $x \sim 10^{-2}$ region which is beyond the reach of fixed-target experiments.

Another independent source of information is direct photon production which is particularly sensitive to the gluon distribution. In addition to the commonly used WA70 data [24], we also include results from the UA6 [25] and E706 [26] experiments. Together these provide coverage of the region $0.27 < x < 0.54$ and, hence, help to constrain the gluon distribution in the middle range of x. The deep inelastic data provide some constraint on the gluon for smaller values of x through the slope of F_2 with respect to Q^2. Additional information at small values of x is provided by direct photon data from various collider experiments. Indeed, the coverage in x extends now down to about 0.02 making a simultaneous analysis of all of the available direct photon data a potentially powerful tool for extracting the gluon distribution. However, there are still unresolved theoretical problems associated with understanding the full range of inclusive (mostly fixed target) and isolated (mostly collider) direct

[4]The resolution of this experimental disagreement lies outside the scope of our work.

photon data which need further study. Such a project has been initiated by members of the CTEQ Collaboration and the results will be presented elsewhere [27]. For the purpose of the present work only the fixed target results on inclusive photon cross-section cited above have been used.

Two new types of data have become available in the past year and they have provided valuable information on PDF's, notably flavor differentiation of partons, which were not fully covered by earlier data sets. In particular, NA51 [11] measured the difference of cross sections for producing lepton pairs at $y = 0$ from proton and neutron targets. As discussed in [28], this is particularly sensitive to the difference of the $\overline{u}$ and $\overline{d}$ distributions. And the CDF Collaboration has presented new data on the charge asymmetry of the decay leptons in W production [10]. This measurement contributes to the differentiation of the valence u and d quarks as well as the sea-quarks. The effects of including these two data sets will be discussed further in the next section.

The full data sets we use are summarized in Table 1.

3 The CTEQ Global Analysis Program

3.1 Global Analysis Procedures

Our goals in the global analysis program are two-fold. On the one hand, we are seeking a universal set of parton distributions which provide an accurate description of all of the data sets and are therefore suitable for use in the calculation of other high energy processes. On the other, we wish to determine to what degree the theoretical treatment of the hard scattering processes in the pQCD framework is consistent with all the available experimental results.

To this end, except where otherwise noted, all data sets included in the analysis are treated on the same footing. This is to be contrasted with an often adopted procedure of emphasizing DIS data as the primary source of information (hence, performing a least-χ^2 fit to these data alone), using the other processes only as supplementary constraints. The simultaneous fitting of many different types of data necessitates the inclusion of both systematic as well as statistical errors. The systematic errors include both overall and point-to-point errors. The treatment of the latter poses a particularly difficult problem. The proper treatment of such errors typically differs from one experiment to another and doing this for all experiments requires a prohibitive amount of computer resources. We studied the impact on the global fit of a full-scale treatment of the (correlated) systematic errors from the high statistics CCFR and BCDMS experiments compared to the common practice of combining the point-to-point systematic and statistical errors in quadrature. The difference is not significant. Thus, we use the latter procedure as an adequate compromise out of practical necessity. (Clearly, a fine-tuning of the final results, including a full treatment of the errors for selected data sets, is possible if necessary.)

The treatment of the overall normalization errors utilized in CTEQ analyses differs from that employed by other groups (including most early PDF's, see [1], and [12]) which usually allow all experimental data sets to be varied freely. In our analysis, with the exception of data which pertain to measured ratios, the normalization (fitting) parameter N_i for each

data set i is associated with a fully correlated error ϵ_i given by the experiment: a term of the form $(1-N_i)^2/\epsilon_i^2$ is then added to the overall χ^2 in the fitting process. This procedure properly takes into account the normalization uncertainties of the experiments, whereas the usual practice mentioned above technically corresponds to assuming infinite normalization errors for all experiments.

The hard cross-sections of all processes included in the analysis are calculated in pQCD to NLO in α_s. We use the $\overline{\rm MS}$ scheme with 5 flavors as the standard, cf. Sec. 3.3 for more details. While such calculations are generally less sensitive than leading-order (LO) results to the choice of the renormalization and factorization scales (denoted jointly by the symbol μ), the residual dependence on these choices provides a potentially important source of theoretical uncertainty. In principle, this uncertainty is one order higher than the approximation used, *i.e.*, next-to-next-to-leading order in our case. In practice, it has been learned that the size of the uncertainty is process-dependent. It is relatively small for DIS and for lepton-pair production and one usually chooses $\mu = Q$, the virtuality of the exchanged virtual vector boson, since this is the natural large scale in the problem. On the other hand, the NLO predictions for direct photon production are still sensitive to the choice of μ. It is important to address this issue if quantitative results on the gluon distribution are to be extracted. The common practice of making a specific choice (say $\mu = p_T$) without discussion implicitly introduces a bias into the analysis because of the non-negligible μ-dependence. In this analysis, we have made the first attempt to address this issue by assigning a "theoretical error" to the predictions associated with the choice of μ. The size of this error is estimated by computing the range of predictions spanned by $\mu = p_T/2$ to $\mu = 2p_T$. During the process of fitting, we let the scale parameter μ for direct photon calculation float and add a contribution to the overall χ^2 due to scale uncertainty given by the deviation of μ from p_T divided by the "error" defined above. Although the details of this procedure (such as the central value for μ and the exact range used to estimate the error) may be the subject of some debate, it nevertheless represents a reasonable treatment of the theoretical uncertainty which otherwise is simply ignored.

3.2 Relation between PDF's and Observables

The relationship between PDF's and the experimental input is in general quite involved since all parton flavors contribute to the NLO formulas for the hard cross-section; and, in addition, the parton distribution functions always mix as the result of QCD evolution. Nonetheless, simple leading order parton model formulas neglecting small sea-quark contributions are often useful in providing a qualitative guide to analysis strategies. We will review the most relevant relations, with the understanding that they are modified by NLO corrections in practice (to varying degrees for different processes).

Consider, first, deep inelastic scattering. The available high statistics data come in four different types, the expressions for which are, in lowest order, given as follows.

$$\begin{aligned} F_2^{\mu p} &= x[4(u+\overline{u})+(d+\overline{d})+2s]/9 \\ F_2^{\mu n} &= x[4(d+\overline{d})+(u+\overline{u})+2s]/9 \\ F_2^{\nu N} = F_2^{\overline{\nu} N} &= x[(u+\overline{u})+(d+\overline{d})+2s] \\ x[F_3^{\nu N}+F_3^{\overline{\nu} N}]/2 &= x[u+d-\overline{u}-\overline{d}] \end{aligned} \tag{1}$$

As noted in [13], these four quantities can be used to extract four combinations of parton distributions, *e.g.,* $u+\overline{u}$, $d+\overline{d}$, s, and $\overline{u}+\overline{d}$, or, equivalently, $u+d$. In particular, these four combinations are sufficient for examining the question of the breaking of SU(3) flavor symmetry of the quark-antiquark sea. Utilizing the equations given above, the strange sea may be expressed as

$$xs = \frac{5}{6}F_2^{\nu N} - 3F_2^{\mu N}. \tag{2}$$

Since the right-hand-side appears as a small difference between two much larger numbers, the relative uncertainty becomes large and, furthermore, is sensitive to the overall systematic errors of the experiments—even though, in recent high precision experiments, the latter have been reduced to a level sufficient for the application of this relation. A more direct measure of the strange quark sea is provided by the ν production of charm. Unfortunately, data on this process have not yet been made available in a form independent of experimental corrections. This issue will be discussed in section 4.1.

The question of SU(2) breaking in the sea is not directly addressed by the types of data listed above. Some information is provided by the Gottfried integral which takes the form

$$I(a,b) = \int_a^b [F_2^{\mu p} - F_2^{\mu n}]\frac{dx}{x}. \tag{3}$$

The NMC Collaboration has measured [29] $I(.004,.8) = 0.236 \pm 0.008$. In lowest order one has

$$I(0,1) = \frac{1}{3} - \frac{2}{3}\int_0^1 (\overline{d}-\overline{u})dx. \tag{4}$$

The experimental result cited above indicates that $\overline{d} > \overline{u}$ when integrated over x. However, information on the x dependence of this SU(2) breaking must be found from another source.

Lepton-pair production (LPP, or the Drell-Yan process) provides direct information on the anti-quark distributions as well as the difference between u and d quarks. For simplicity, consider the cross-section

$$\frac{d\sigma}{dQ^2dy}|_{y=0} \tag{5}$$

for LPP in proton collisions on an isoscalar target. In lowest order, retaining only the light quark and antiquark contributions, this cross section is proportional to the following product of parton distributions:

$$\Sigma_{\mu\mu} = (4u+d)(\overline{u}+\overline{d}) + (4\overline{u}+\overline{d})(u+d) \tag{6}$$

where each of the distributions is evaluated at $x = Q/\sqrt{s}$. Note that all terms on the right-hand side are directly proportional to anti-quark distributions (in contrast to DIS where $\bar{q}(x)$ usually is submerged under $q(x)$ for a large part of the x-range). Eq.(6) can be rewritten as

$$\Sigma_{\mu\mu} = 5(\overline{u}+\overline{d})(u+d) + \frac{3}{2}(\overline{u}+\overline{d})[(u+\overline{u})-(d+\overline{d})] + \frac{3}{2}(\overline{u}-\overline{d})[(u+d)-(\overline{u}+\overline{d})]. \tag{7}$$

In principle, all of the terms except $(\overline{u}-\overline{d})$ are constrained by the deep inelastic data. Therefore, the lepton pair data provide a direct measure of the SU(2) breaking of the sea, *i.e.* $(\overline{u}-\overline{d})$, when used in conjunction with the deep inelastic data. In fact, the E-605 data

on $d^2\sigma/dQ^2dy$ used in this analysis cover a range in y (centered about zero). This provides even more information than the $y = 0$ case shown above – since the y-dependence extends the x range through the relation $x_{1,2} = \sqrt{Q^2/se^{\pm y}}$ – but the principle is the same.

All the CTEQ analyses result in substantial SU(2) breaking due to the use of the full range of DIS and LPP data. Since the E-605 data constrain the PDF's over a range in x covering approximately 0.10 - 0.6 (when the y-range is taken into account), the SU(2) breaking effects observed are reliable only over this range. To extend these results to lower values of x, additional experimental measurements will be needed.

Recently, the NA51 experiment[11] measured the asymmetry between the cross section for producing lepton pairs from proton and neutron targets, designed to probe directly the quantity $(\overline{u} - \overline{d})$. As shown in [28], this quantity can be written as

$$A_{DY} = \frac{(4u_v - d_v)(\overline{u} - \overline{d}) + (u_v - d_v)(4\overline{u} - \overline{d})}{(4u_v + d_v)(\overline{u} + \overline{d}) + (u_v + d_v)(4\overline{u} + \overline{d})} \tag{8}$$

where the subscript v denotes a valence distribution. The NA51 result is $A_{DY} = -0.09 \pm 0.028$ at $y = 0$ and $Q/\sqrt{s} = 0.18$, where the statistical and systematic errors have been added in quadrature. Comparison with Eq.(8) shows that since $u_v/d_v \approx 2$, one must have $\overline{u} < \overline{d}$. This is consistent with the sign of the breaking indicated by the Gottfried sum result.

Also of interest is the lepton charge asymmetry recently observed in W production by the CDF Collaboration. Consider the charge asymmetry of W production (before decaying into leptons), defined as

$$A_W(y) = \frac{d\sigma^+/dy - d\sigma^-/dy}{d\sigma^+/dy + d\sigma^-/dy} \tag{9}$$

where the superscript denotes the charge of the W. For $\overline{p}p$ collisions in leading order parton model, $A_W(y)$ is given approximately by

$$A_W(y) \approx \frac{u(x_1)d(x_2) - d(x_1)u(x_2)}{u(x_1)d(x_2) + d(x_1)u(x_2)} \tag{10}$$

where $x_{1,2} = x_0 e^{\pm y}$ and $x_0 = M_w/\sqrt{s}$. Letting $R_{du} = d/u$, one can write

$$A_W(y) = \frac{R_{du}(x_2) - R_{du}(x_1)}{R_{du}(x_2) + R_{du}(x_1)}. \tag{11}$$

As noted in Ref.[28], in the region of small y (where $R_{du}(x_1) \approx R_{du}(x_2) \approx R_{du}(x_0)$) this asymmetry is directly proportional to the *slope of the ratio* R_{du} in x:

$$A_W(y) \approx -x_0 y \frac{dR_{du}}{dx}(x_0)/R_{du}(x_0). \tag{12}$$

For the CDF experiment, $x_0 = 0.044$ and $|y| < 2$, thereby providing information on the ratio of the d and u distributions in the region of x of $(0.01, 0.2)$. Actual data on this process are for the corresponding decaying lepton asymmetry, so the above discussion is relevant only on the qualitative level since Eqs.(10-12) are considerably smeared when applied to the measured leptons.

As mentioned earlier, in addition to these simple parton model relations, some observables can be sensitive to parton distributions through NLO effects. Two examples come readily to mind: the precise data on DIS place important constraints on the gluon distribution $g(x,Q)$ in the region $x < 0.2$ (not covered by current fixed-target direct-photon data) through the Q-dependence of the structure functions; and LPP data provide additional constraints on $g(x,Q)$ through the "Compton-scattering" mechanism. These examples caution us against taking simple parton relations too literally under all circumstances.

3.3 Choice of Parametrization

We now address the issue of the parametrization of the initial PDF's at some Q_0 which serves as the non-perturbative input to the global analysis. The forms chosen must be flexible enough to account for all experimental input, if possible, yet they should not be under-constrained. Considering the current status of the experimental evidence as discussed above, the parametrization must allow for breaking of both SU(3) and SU(2) flavor symmetry. Our input parton distributions are parametrized at $Q_0 = 1.6$ GeV (which coincides which the charm threshold we use, see below). The Q-dependence of the parton distributions is generated by QCD-evolution using two-loop expressions for the splitting functions and running coupling. In general, the $\overline{\rm MS}$ factorization scheme is used although, in response to the need for DIS-scheme and leading-order (LO) calculations, we also generate equivalent parton distributions in these schemes. The heavy quark thresholds are taken as 1.6 and 5.0 GeV for the c and b quarks, respectively, and the heavy quark distributions are generated using massless evolution starting from a boundary condition of a vanishing PDF at the appropriate threshold equal to the corresponding quark mass. The renormalization scheme on which this definition of heavy quark parton distribution functions is based has been formulated precisely in Refs.[30, 31]. In principle, it is possible to have non-zero heavy-quark distributions at threshold – *e.g.* to have some "intrinsic charm", as has been suggested occasionally in the literature. We do not include this possibility for lack of positive experimental evidence at this time.

The functional forms used for the initial parton distributions in the three rounds of CTEQ analyses vary slightly. We give here the explicit expressions used in the most current CTEQ3 analysis:

$$\begin{aligned}
x u_v &= a_0^u x^{a_1^u}(1-x)^{a_2^u}(1+a_3^u x^{a_4^u}) \\
x d_v &= a_0^d x^{a_1^d}(1-x)^{a_2^d}(1+a_3^d x^{a_4^d}) \\
x g &= a_0^g x^{a_1^g}(1-x)^{a_2^g}(1+a_3^g x) \\
x(\overline{d}+\overline{u})/2 &= a_0^+ x^{a_1^+}(1-x)^{a_2^+}(1+a_3^+ x) \\
x(\overline{d}-\overline{u}) &= a_0^- x^{a_1^-}(1-x)^{a_2^-}(1+a_3^- x) \\
x s &= \kappa \cdot x(\overline{d}+\overline{u})/2
\end{aligned} \tag{13}$$

The coefficients a_0^u and a_0^d are fixed by the number sum rules for the valence quarks[5] and the gluon normalization coefficient a_0^g is fixed by momentum conservation. Furthermore, with the data currently available it is not possible to separately determine the low-x behavior for the sea and gluon distributions, so we have chosen $a_1^g = a_1^+$ and set the strange quark

[5]For our choice of functional form, Eq. 13, a_0^u and a_0^d can be expressed as combinations of Euler Beta functions, *e.g.* $a_0^u = 2/[B(a_1^u, a_2^u+1) + a_3^u B(a_1^u, a_2^u+a_4^u+1)]$.

distribution to be proportional to the average non-strange sea. We have also fixed $\kappa = 1/2$ in most of our fits since the resulting $s(x, Q_0)$ agrees well with the recently published NLO strange quark distribution measured in the most accurate dimuon neutrino experiment [32]. (Deviations from these choices used in earlier CTEQ1 and CTEQ2 analyses will be noted in the next section.) Further reduction of independent parameters could be achieved by assumptions such as $a_1^u = a_1^d = a_1^-$ (motivated by Regge exchange considerations). The viability of such assumptions needs to be tested during the process of the global analysis.

In practice, the series of CTEQ analyses adopted the procedure of starting with a sufficient number of parameters to establish a good fit, then systematically reducing that number to eliminate extraneous degrees of freedom while maintaining good agreement with data. In the most recent CTEQ analyses we found it possible to obtain excellent overall fit using only 15 independently adjustable *shape parameters* to describe the input distributions (see Sec. 4.3 and Table 3 for details). In addition, there are individual normalization parameters for each experiment (constrained by appropriate experimental errors, as described earlier), the value of Λ_{QCD}, and the value of the parameter associated with the theoretical scale uncertainty in direct photon calculations discussed in Sec.3.1.

Applying the PDF's obtained here to generate predictions for processes at new facilities in regions of x and Q^2 beyond those covered in the current global analyses necessarily entails extrapolations in these variables. If one is interested in a region of x below that which was fitted, but at a higher value of Q^2, the "feed down" property of the evolution equations (due to the parton splitting process) provides reasonably reliable extrapolations (cf. [1]) – provided the input distribution functions in this x region are relatively smooth (hence the result is dominated by the nature of the splitting kernel). On the other hand, if one is interested in small x and moderate Q^2, where the PDF's are still dominated by the input functions, the results are in fact only extrapolations, not constrained either by theory or experiment. It is thus important to chose functional forms that smoothly extrapolate into such regions while simultaneously acknowledging the inherent risk of such extrapolations. Sometimes, a given functional form can lead to unintended behavior of the parton distributions beyond the region where data exist. These considerations must be kept in mind, as the parametrization of the non-perturbative initial parton distributions, although guided by certain qualitative "theoretical considerations"(many of which have had to be abandoned in recent years in the face of new experimental results), is ultimately dictated by data and by experience gained in previous global analyses.

The choices shown above are certainly not unique and do, in fact, differ slightly from those used in other work, both by us and by other groups [13]. It is possible to generate fits of comparable quality (in the sense of least-χ^2) using somewhat different functional forms as long as both forms can parametrize the requisite parton distribution shapes to account for current data. In that case, any remaining difference in the parton distributions can only be resolved by future experiments.[6]

[6] A detailed study of this issue under current experimental conditions will be reported in a separate paper.

4 Results on Parton Distributions

Three rounds of global analysis based on the general procedures described above have been completed by the CTEQ collaboration. A short report on the CTEQ1 analysis has already been published [6]. Aside from obtaining several up-to-date sets of parton distributions (the "CTEQ1 distributions"), this analysis uncovered an unexpected inconsistency among existing experiments concerning the flavor dependence of the sea quark distributions. We briefly discuss the relevant points and subsequent developments on this issue in the next subsection. The advent of new data from HERA along with an alternative treatment of the strange sea led to the development of the CTEQ2 distributions which were made available in the Fall of 1993. These distributions are described in Sec. 4.2. Recent lepton pair asymmetry data from NA51 and W-decay lepton asymmetry data from CDF prompted refinements of the analysis, resulting in a new set of CTEQ3 distributions which we discuss in detail in Sec. 4.3.[7] Comparisons with other distributions are presented in Sec.5.

4.1 CTEQ1 Parton Distributions

The CTEQ1 analysis [6] was based on data on cross-sections and structure functions available at the end of 1992. The list of data sets used is given in Table 1 with "1" marked in the final column. Very good fits to this wide range of data were obtained—both the overall χ^2 and the χ^2 distribution among the experimental data sets indicate a remarkable degree of consistency and are in much better quantitative agreement with the available data than previous global fits. Five sets of parton distributions representing two best fits in the $\overline{MS}$ and DIS scheme (CTEQ1M and CTEQ1D), one fit with a "singular" gluon distribution (CTEQ1MS), one with Λ_{QCD} fixed at a higher ("LEP") value (CTEQ1ML), and one suitable for leading order calculations (CTEQ1L) were obtained. See Ref. [6] for details.

One disturbing feature of the CTEQ1 parton distributions was that the strange quark distribution $s(x,Q)$ obtained was considerably larger in the $x < 0.1$ region then those obtained from leading-order parton model analysis of the neutrino dimuon production data [33, 34, 35]. It was pointed out that this $s(x,Q)$ behavior follows necessarily from the high precision input data sets on total inclusive structure functions measured by the CCFR and NMC collaborations through the familiar ("charge ratio") parton model identity $\frac{5}{6}F_2^{\nu N} - 3F_2^{\mu N} = s(x,Q) +$ *small corrections*, cf. Eq.(2). As remarked earlier, although this combination of structure functions entails using the (small) difference between two larger numbers, the quoted experimental statistical and systematic errors of the relevant high precision DIS experiments are even smaller, hence enabling this relation (which is implicitly embedded in the global analysis calculations) to play a decisive role in the determination of $s(x,Q)$.

The apparent disagreement with the dimuon results on $s(x,Q)$ imply either the theoretical input (to the global analysis or to the dimuon analysis) has deficiencies, or some experimental data sets are inconsistent with each other within the quoted errors. Although our global analysis, by itself, cannot resolve this dilemma, it was the insistence on taking available data and their quoted errors seriously which resulted in uncovering this controversial issue.[8]

[7] Computer programs for generating all the CTEQ parton distributions described below are available from H.L. Lai (Lai_H@msupa.pa.msu.edu) or W.K. Tung (Tung@msupa.pa.msu.edu) upon request.

[8] To avoid this inconsistency, one has to either arbitrarily enlarge the quoted experimental errors or

Ref. [6] suggested careful examination of all possible theoretical and experimental sources of this disagreement. Subsequently, CCFR has reanalyzed their dimuon data [32] using the NLO formalism of [36, 31] (which is more consistent with our theoretical framework), resulting in a modified strange quark distribution. Nonetheless, the above disagreement persists.

On the theory side, the treatment of heavy quark production channels in the total inclusive structure functions $F_{2,3}^{\nu N}$ and $F_2^{\mu N}$ in all existing global analysis work is done using the familiar zero-mass formalism plus a leading-order "slow-rescaling" correction prescription — hence is not truly consistent with the overall NLO and dimuon analyses. A proper method to treat this problem now exists, cf. Refs.[36, 31]. The implementation of this improved theoretical calculation is underway by the CTEQ group.

On the experimental front, there is considerable sentiment that information obtained on $s(x, Q)$ from neutrino dimuon data should be more reliable than that from the difference of $F_2^{\nu N}$ and $F_2^{\mu N}$ obtained in total inclusive measurements —in spite of the quoted errors. If this is the case, then there exists some inconsistency in currently available data on $F_2^{\nu N}$ and $F_2^{\mu N}$ in the $0.01 < x < 0.1$ region [37],[38]. At least one of these data sets needs to be reassessed, particularly concerning systematic errors.

The neutrino dimuon results were not included in the CTEQ1 analysis because experimental data in this process are not, so far, available in the form of detector-independent physical quantities (i.e. structure functions) which can be included in a global analysis treating all data on the same footing. In view of the resulting inconsistency, the CTEQ2 analysis takes the complementary approach of making direct use of the strange quark distribution function obtained by the CCFR collaboration from their parton model analysis of the dimuon data, thereby setting this process apart from all the other experimental input. Obviously, neither approach is completely satisfactory. Eventually, we need to understand the source of the inconsistency, and perform a consistent global analysis including measured dimuon structure functions, thereby avoiding a separate treatment of the strange quark.

There is another process which is potentially sensitive to the size of the strange sea. $W-$boson plus charm associated production at hadron colliders involves a term which is directly proportional to the strange quark sea. Estimates for this process show that it may be possible to provide some limits on the strange/non-strange ratio as further data are accumulated [39]. In addition, a next-to-leading-order calculation of this process is in progress [40].

4.2 CTEQ2 Parton Distributions

The CTEQ2 analysis was initiated after the first measurement of $F_2^{ep}(x, Q)$ from HERA became available [9]. These new data not only extended the measured range of x by two orders of magnitude; they also offered the possibility of formulating the global analysis in an alternative way in the face of the dilemma exposed by the CTEQ1 study. The HERA data provide very useful constraints on the small-x behavior of the parton distributions even with their relatively large initial errors because of the extended reach down to $x \sim 10^{-4}$. We therefore modified the input used in the CTEQ1 analysis by adding the new HERA

overlook (and accept) statistically significant inconsistent fits.

data in conjunction with: (i) using a parametrized function $s(x, Q_0)$ obtained by the CCFR collaboration in NLO QCD analysis which was allowed to vary within an error band provided by the experiment [32]; (ii) removing the conflicting CCFR and NMC F_2 data between $x = .01$ and $x = .09$ which forced the large strange sea through the charge ratio relation, Eq.(2), in the previous analysis; (iii) including the same fixed-target lepton-pair and direct photon production data sets; and (iv) adding the new collider data on lepton-pair production obtained by CDF[23]. The full list of experiments appears in Table 1 with the last column marked either 1 or 2.

We obtained global fits to the experimental data mentioned above, again, with remarkable consistency over all data sets. (See Table 4 for detailed information on χ^2 distributions.) Six representative sets of parton distributions were selected for use in applications. Following the general CTEQ convention, they are designated as CTEQ2M, CTEQ2MS, CTEQ2MF, CTEQ2ML (for $\overline{MS}$ best fit, Singular, Flat, and *LEP*-Λ respectively)[9], CTEQ2L (Leading order best fit), and CTEQ2D (DIS scheme best fit). The parameters for the initial distribution functions are given in Table 2.

In comparison to recent experimental data not included in the fit, the CTEQ2 prediction for the charge asymmetry in lepton-pair production A_{DY}, cf. Eq.(8), is small and negative — in qualitative agreement with the new NA51 data.[11] This is shown in Fig.1.[10] As discussed in Sec. 3.2, our use of the full set of double differential cross-section $d^2\sigma/dQ^2dy$ measured by the E605 experiment already constrained the $\bar{d} - \bar{u}$ distribution in the $0.1 < x < 0.5$ region. Thus, the (slightly over 1 σ) agreement of the CTEQ2 result with the new NA51 data point can be regarded as a reasonable consistency check. (Other work on parton distributions tend to use the less comprehensive single differential LPP cross-section $d\sigma/dQ^2$ as a constraint on fits which include only DIS data, hence do not take advantage of the full power of the complete E605 data set.)

On the other hand, the recently measured lepton asymmetry in W-production $A_W(y)$, cf. Eq.(9), by CDF conveyed a different message. It was observed that the predictions of the CTEQ2 distributions were consistently higher than the data, as shown in Fig.2. (cf. footnote 10.) Since $A_W(y)$ depends on the x-variation of the ratio d/u, as discussed in Sec.3.2, one naturally turns to data on the ratio of F_2^p/F_2^n in DIS (which also depends on d/u) for a consistency check. It turns out that the CTEQ2 distributions provide an excellent description of the full set of high precision NMC data on F_2^p/F_2^n. In fact, a careful study of the quality of fits to all experimental data sets (cf. Table 4) of the CTEQ2 distributions compared to that of other contemporary distributions reveals that CTEQ2 gives a much better overall fit (at least in terms of a substantially lower χ^2)[11] even if others may agree with the specific $A_W(y)$ measurement better. This underlines the fact that $A_W(y)$ is particularly sensitive

[9] To be specific: CTEQ2MS (CTEQ2MF) assumes a *singular (flat)* small-x behavior of the form $xf(x, Q_0) \sim x^{-0.5}$ (x^0) for the sea quarks and gluons; and CTEQ2ML fixes Λ_5 at 220 MeV. For comparison, the *standard* CTEQ2M has $xf(x, Q_0) \sim x^{-0.26}$ and $\Lambda_5 = 139$ MeV.

[10] The other curves in this figure are obtained from the new CTEQ3M distributions (to be described in the next subsection) and from the two recent generations of MRS distributions. Comparisons of these will be discussed later.

[11] To be specific: using our treatment of experimental errors (close to those specified by the experiments in all cases), the difference in χ^2 is of the order 80-90 (for 920 points) which are evenly distributed in one of the high precision DIS experiments, either BCDMS or CCFR .

to *one aspect* of the PDF's – the *slope* of d/u (cf. Sec.3.2) – which is not probed by the other experiments. To study the implication of this fact, we should ask then: Is it possible to vary the CTEQ2 distributions to fit the $A_W(y)$ data and, at the same time, maintain the same quality of agreement with all the other experiments? Or, can we reconcile and understand the interplay of all experiments which play a role in flavor differentiation of the u and d quarks —F_2^p/F_2^n, E605, $A_W(y)$ and NA51? This question will be addressed in the next section on CTEQ3 analysis.

One may note that the results in Table 4 reveal that the overall χ^2 value in the global fit (including the new data sets mentioned above) for CTEQ2M remains the *lowest* even compared to the two more recent fits which are designed to give better description of the new data. This fact serves as a reminder that total χ^2 is not necessarily the best or only measure of a "good fit" in a global analysis. The balanced distribution of χ^2's among data sets, particularly those which are sensitive to specific features – such as the $A_W(y)$ measurement to the d/u ratio (relevant for SU(2) flavor differentiation) – must also be taken into account. The new CTEQ3 distributions give a more balanced fit in this sense at the expense of marginally higher total χ^2; hence, they represent an improved general purpose parton distribution set.

Since the CTEQ2 distributions do give such a good global fit to the full data set, the fine-tuning which leads to CTEQ3 only entails very small shifts in the u and d quark distributions, as will be shown in the next two sections. Consequently, for the vast majority of applications which are not sensitive to the precise distinction between u and d quarks, there will hardly be any observable differences in practice. In particular, the special CTEQ2 distributions designed to test specific assumptions, such as CTEQ2MF (flat) and CTEQ2MS (singular) to map out a range of small-x behavior which bracket the HERA data (cf. Fig.3) and CTEQ2ML (large-lambda) which has a higher value of Λ with a somewhat different gluon distribution, remain perfectly valid for their original purposes.

4.3 CTEQ3 Analysis and Distributions

Previous global analyses have been dominated by experimental data collected at fixed-target energies. The observed sensitivity of the new CDF data on $A_W(y)$ to details of the parton distributions, particularly u and d quarks, ushers in a new stage of global analysis marked by an increasing role for quantitative measurements at hadron colliders.[12] In addition, with the increased number of physical processes included in the analysis, we are approaching the point where all parton flavors will be sufficiently constrained to lead to either an (almost) unique set of PDF's (in the x range covered by the experiments) or evidence for potential inconsistencies. The detailed CTEQ3 analysis is undertaken to respond to this new development and to address the related issues discussed at the end of the last subsection. All data sets listed in Table 1, including the recent NA51 and CDF $A_W(y)$ measurements and the final 1994 ZEUS data on $F_2(x,Q)$[41], are included in the global fit.

The specific parametrizations for the initial parton distributions (at $Q_0 = m_c = 1.6\,\mathrm{GeV}$) used in this analysis are discussed in Sec.3.3. The effect of various choices of functional

[12] Other measurements which will soon play an important role, especially for probing the gluons, are precise data on direct photon production (including photon plus jet) and jet cross-sections (including di-jets).

forms and the number of independent parton shape parameters on the predicted behavior of the various processes and on the global analysis have been extensively studied. We found that: the new data do help constrain the flavor dependence of the quark distributions, in particular the u and d, much better then before. From these studies, we have chosen a representative set of new parton distributions – the CTEQ3 distributions, which give a best balanced fit to all available data. Details will be described below. In the next section, we compare these PDF's with other available sets and with representative experimental data sets. Unresolved issues and assessment on uncertainties of the PDF's which emerge from this round of detailed analysis will be discussed in the Sec.6.

Following the general CTEQ convention, the new parton distribution sets in the commonly used factorization schemes will be referred to as CTEQ3M ($\overline{\rm MS}$), CTEQ3D (DIS), and CTEQ3L (Leading-order) respectively. These three sets are obtained from independent fits to the same data sets under the same assumptions except the scheme for calculating the evolution kernel and the hard cross-sections. Thus, they are *functionally equivalent* in the sense that (when applied in the appropriate scheme) they yield the same physical cross-sections, within errors, for the data included in the analysis; they are, however, not *algebraically equivalent* in the sense that they could be obtained from each other by applying the applicable perturbative transformation formula between the schemes. The latter is known to be unreliable in many situations where nominal NLO terms (e.g. those involving a large gluon contribution) are of comparable numerical size as the LO term (e.g. involving small sea-quarks). In the ensuing discussions, we shall only mention the CTEQ3M distributions explicitly.

The parton distribution shape parameters at $Q_0 = 1.6$ GeV for the CTEQ3 distributions obtained from the global fit are listed in Table 3. During the process of this analysis, we started from the full set of (18) parameters introduced in Sec.3.3, then tried to systematically reduce the number of independent parameters while maintaining the quality of the fit as established by benchmarks from the starting fits. The final fit involves 15 parton shape parameters, which is considerably lower than the previous CTEQ analyses, and also lower then the current MRSA one.

The total χ^2 is 839 for 850 degrees of freedom, using the data sets listed in Table 1. The distribution of the χ^2 values among the various processes and data sets is balanced, as summarized in Table 4 which also show the corresponding χ^2 values obtained for some other parton distribution sets (representing both the current and the previous generation of PDF's) in order to indicate where the differences between the various sets lie, as already mentioned in the last subsection. The normalization factors for the various experiments emerging from the CTEQ3 global fit are given in Table 5.

To illustrate the quality of the fit, we present in Fig.4 the comparison with BCDMS and NMC data on muon $F_2^p(x,Q)$[13]; in Fig.5 the NMC data on F_2^p/F_2^n; in Figs.6 & 7 the CCFR data on neutrino F_2 and F_3 (cf. footnote 13); in Fig.8 the latest ZEUS data on F_2^p; in Fig.9 the double differential lepton-pair data of E605; in Fig.10 the combined direct photon data at $y \sim 0$ from E706, UA6, and WA70. The various data sets appearing on the same plot in

[13]As mentioned in Secs. 4.1 and 4.2, data points from CCFR and NMC structure functions (but not the ratio F_2^p/F_2^n) have been excluded in the analysis, hence are not shown in these plots. Comparison of the excluded data points with the resulting fit will be discussed in Sec. 6, cf. Fig. 23.

all these figures have been multiplied by offset factors to avoid overlap; hence the vertical scales are in arbitrary units and they are not labelled. The "goodness of fit" represented by the χ^2 table is made explicit by these plots. Comparison to the NA51 data point on lepton-pair charge asymmetry was shown earlier in Fig.1, Sec.4.2; and comparison to the CDF W-lepton asymmetry data was shown in Fig.2 in Sec. 4.2.

An overview of the various flavors of CTEQ3M parton distributions at the scale $Q = 5$ GeV is displayed in Fig.11. Included (near the bottom of the figure) is the difference between $\bar{d}$ and $\bar{u}$ distributions, which has been a subject of much attention in the last few years. The fact that we can now investigate quantitatively the behavior of such a small difference illustrates the significant progress made possible by recent high precision experiments and accurate calculations. We will discuss the uncertainty on this difference later.

Concerning the global analysis which lead to the CTEQ3 parton distributions, we notice that:

∘ The value of $\Lambda^{5\ fl}_{QCD}$ —158 MeV, obtained in this round of analysis (cf. Table 3), is similar to the values obtained in previous global fits. It corresponds to a value of $\alpha_s(M_Z^2)$=0.112, in agreement with the value determined from Q-dependence of DIS structure functions, but lower than that from global analysis of LEP data [42], reflecting again the dominance of DIS in the current global analysis. However, since the value of Λ. is correlated with other parameters in the global fit, particularly those associated with gluon shape which may not be well-determined yet, there is still a range of uncertainty on Λ. We found that alternative ways of treating certain processes, e.g. using a particular fixed scale in direct photon calculations, can cause Λ to shift (usually to higher values) by 30-40 MeV.

∘ The reach into the small-x ($10^{-2} - 10^{-4}$) range, and the recent reduction in errors, provided by the HERA experiments put rather stringent constraints on the effective power a_1 ($-0.35 < a_1 < -0.25$) for the sea quarks, cf. Eq. (13). The need to vary this parameter over a certain assumed range, as done in the past, has diminished. To show the progression of development, Fig.3 plots the recent ZEUS data on F_2 as a function of x at $Q^2 = 15$ GeV^2 compared to CTEQ3M and some previous distribution sets which assume $a_1 = 0$ (MRSD0', CTEQ2MF) or $a_1 = -0.5$ (MRSD-', CTEQ2MS), and which either came before the advent of any HERA data (MRSD) or were constrained by the early HERA data (CTEQ2). We see that the MRSD distributions are now away from current data; whereas the two CTEQ2 sets now bracket the new data points (rather than "fit" them).

It is important to bear in mind that the values quoted for a_1 from our fit, as for others, is applicable at the specified scale Q_0 only (1.6 GeV for CTEQ3). The evolution of the parton distributions with increasing scale to an ever softer (i.e. singular) shape will cause this effective power to increase in absolute value. Thus, comparison with "theoretical expectations" of small-x behavior for fixed (but unspecified) Q, such as those from the BFKL hard pomeron [43], is inherently of limited validity.

∘ A new feature of the CTEQ3 (and CTEQ2) analysis is the inclusion of a theoretical parameter representing the uncertainty associated with the choice of scale in direct photon calculations (cf. Sec.3.1). The best estimate of this parameter which gives the optimal overall fit is in the range $\mu/p_T = (0.4 - 0.5)$ which is quite reasonable.

Unlike in the past, where within the $\overline{\rm MS}$ scheme some alternative sets reflecting certain

uncertainties[14] were also given, we have restricted the CTEQ3 distributions to the three equivalent sets (3M, 3D and 3L) mentioned above since: (i) these uncertainties are steadily decreasing as progress is been made; and (ii) as discussed in the last subsection, for making comparative studies, the alternative CTEQ2 parton sets (2MF, 2MS & 2ML) still serve the original purposes quite adequately, as the transition to the new version only entails certain fine-tuning which does not affect those purposes (e.g. see Fig. 3 and the discussion on small-x behavior above).

5 Comparisons of Parton Distributions and Recent measurements

To see the status of global QCD analysis and the recent progress, we compare the CTEQ3M parton distributions to the current MRSA set and to the earlier CTEQ2M and MRSD-' sets. We limit the comparison to these parton distribution sets since they have been determined in a program comparable in scope to that which has been described here.

Figs.12-17 display the $u_v(x,Q)$, $d_v(x,Q)$, $g(x,Q)$, $\bar{u}(x,Q)$, $\bar{d}(x,Q)$, $s(x,Q)$ distributions respectively from the four sets of PDF's at $Q = 5$ GeV in the range $10^{-4} < x < 0.8$. We observe that:

∘ The small spread between the previous generation CTEQ2M and MRSD-' valence quarks (curves with dots in Figs.12 & 13) has been noticeably narrowed in the current round of analyses given by CTEQ3M (solid) and MRSA (dashed). The $u_v(x,Q)$ and $d_v(x,Q)$ distributions are now very well determined indeed throughout the range where they are not vanishingly small.

∘ As shown in Fig.14, the gluon distributions from the three sets incorporating HERA data in the fit – CTEQ2M, CTEQ3M and MRSA – are also in close agreement. The more singular behavior of MRSD-' is due to the input condition without the benefit of data. We will discuss the uncertainty on the gluon distribution later in Sec. 6.

∘ For the $\bar{u}(x,Q)$ and $\bar{d}(x,Q)$ distributions, shown in Fig.15 and Fig.16, the MRSA distributions are somewhat higher than the CTEQ ones, even though they are both determined mostly by the same HERA data. The reason lies mainly with the different normalization factors used by the different fits. (Cf. Table 5.) This difference arises from the different ways the two groups treat experimental uncertainties, especially the normalization, in their respective fits (cf. detailed discussion in Sec.3.1); and it is also influenced by our exclusion of the controversial CCFR and NMC data points below $x = 0.09$.

∘ The differences in the strange distribution, shown in Fig.17, are entirely due to differences in input assumptions. The CTEQ2M input distribution is taken from the $s(x,Q)$ distribution furnished by the recent CCFR experiment on neutrino dimuon production [32]; the other three used the constraint $s(x,Q) = (\bar{u}(x,Q) + \bar{d}(x,Q))/4$ which is consistent with the above data, within errors, in the measured range $0.015 < x < 0.3$. The small-x extrapolations follow the functional forms assumed.

We now discuss briefly the comparison of recent NA51 and CDF charge asymmetry data

[14]Such as small-x behavior and the value of Λ_{QCD} (e.g. CTEQ2MS, CTEQ2MF, and CTEQ2ML).

which motivated the new round of analyses with results obtained from these distributions. The new parton distributions MRSA and CTEQ3M use these data as part of the input and, hence, their agreement with data is expected. It only remains to understand the changes these new data brought about in the parton distributions.

In Fig.1 the result [11] for A_{DY} is compared to the results of different fits. Although the data set only consists of one single point, it obviously has a major impact on the MRS analyses. The effect on CTEQ analysis is less dramatic (for reasons discussed in Sec.4.2), but still substantial. Fig. 2 shows a comparison of the same fits to the W decay lepton asymmetry data [10] on A_W . The impact here is mainly on the CTEQ analyses with the much improved agreement of the CTEQ3M distributions compared to the CTEQ2M distributions. Both MRS sets fit this data set well.

Although long-established DIS data on proton and nuclear targets, along with lepton-pair production data provide the main source of information on the u and d quarks, these two recent experiments played a surprisingly significant role in pinning down the details of the distinction between the two lightest quark flavors. As discussed earlier in Sec.3.2, A_{DY} is mainly sensitive to the difference $(\overline{d}-\overline{u})$, whereas A_W is most sensitive to the x-dependence of the ratio d/u which includes both valence and sea. Hence, we show in Fig.18 and Fig.19 the comparison of these combinations of parton distributions from the four sets of distributions respectively. The plot of $(\overline{d}-\overline{u})$ in Fig.18 is the most dramatic in demonstrating the change of our knowledge on parton distributions brought about by these recent experiments. The large movement of MRSD-' curve toward MRSA is forced by the NA51 data. The change of CTEQ2M curve toward CTEQ3M is influenced by the adjustments needed to fit the A_W data, mainly in the region around $x = 0.05$.[15] The d/u plot of Fig.19 does not display a significant difference in the four curves. Nonetheless, close examination of the differences in the slope of these curves in the region $0.02 < x < 0.2$ does bear out the expectations discussed in Sec.3.2.

6 Uncertainties and Challenges

Since the existing experimental and theoretical input to global QCD analyses are not quite sufficiently extensive and accurate to determine a unique set of parton distributions, it is useful to have some feeling about the uncertainties of the PDF sets. The common practice of assigning uncertainties according to the spread of some chosen subset of currently available distributions is quite haphazard, as most published sets are selected out of many possible candidates; and as PDF's obtained by different groups are not always comparable because they are based on different assumptions and inputs. A comprehensive program to systematically assess the uncertainties of PDF's based on error matrix analysis is a desirable goal, but rather difficult because of the complexity of the global system. It is certainly not presently available. In this section, we state the outstanding problems in the determination of parton distributions and describe in qualitative terms the current uncertainties based on extensive exploratory work done by the CTEQ group beyond that contained in the three rounds of specific parton distribution sets bearing the collaboration label. We also comment on the

[15] The reduction of one parameter in the input functional form for $(\overline{d}-\overline{u})$ from CTEQ2 to CTEQ3 also has some influence in the change.

origin of the observed good agreement as well as some of the minor differences between the current generation of MRSA and CTEQ3 distributions in order to address the question: to what extent do these agreements and differences reflect real current uncertainties on the parton distributions?

◦ **The gluon distribution:** It is common knowledge that the best available handles on the gluon distribution are the Q-dependence of the DIS structure functions and cross-sections for direct photon production, although it affects all QCD processes—at least through evolution of all parton distributions and NLO hard cross-sections. These two processes complements each other. The DIS data are quite precise; but the measurement is "indirect" (i.e. through QCD evolution only) – hence it is applicable only in the smaller x-region where the influence of the gluon distribution on the measured structure functions can be seen. The direct photon measurement is "direct" but, so far, available data still have large errors and theoretical uncertainties are greater. The "good agreement" between the CTEQ and MRS gluon distributions shown in Fig. 14 is not evidence for a well-determined $G(x, Q)$, it merely reflects the common assumptions made by the two groups. For instance, the agreement below, say $x \sim 0.05$, can be attributed to the fact that the most important gluon shape parameter which governs its small-x behavior – a_1 in the factor x^{a_1} (cf. Eq.(13)) – is assumed to be the same as that of all the sea-quarks (which is rather well determined by the new HERA data) by both. This is only an assumption. To assess uncertainties, we need to go beyond the standard sets.

For moderately large x, $G(x, Q)$ should be determined by the direct photon data used in the global analysis. Fig.20a displays the gluon distributions in the range $0.1 < x < 0.6$ at $Q = 5$ GeV from CTEQ3, MRSA and the alternative CTEQ2 sets which were designed to explore some aspects of parton distribution uncertainties. The CTEQ2ML set (with a larger Λ value which is closely correlated to gluon behavior) and the CTEQ2MS & CTEQ2MF sets (with a different small-x behavior which affects all x-ranges by the momentum sum rule) give a better indication of the range of possible gluon behavior. The CTEQ analyses used all available fixed-target photon data sets – WA70, E706, and UA6. We see that the range of variations are fairly large. This is because both point-to-point and overall normalization errors on all these data are still large, and theoretical uncertainties (partially taken into account in the CTEQ analyses) are not yet under full control.

The behavior of $G(x, Q)$ in the small-x region is a wide open problem. Under the commonly made assumption that the a_1 parameter for the gluon is the same as for the sea quarks, Fig. 20b show the same gluon distribution sets as above over the extended range $10^{-4} < x < 0.6$. Since CTEQ2MF and CTEQ2MS envelop the current HERA data in the small-x range, this plot gives a reasonable representation of the uncertainty under the given assumption. However, the possibility that the gluon distribution may have a different behavior must be kept in mind unless it is ruled out by future experiment.

More detailed analysis of direct photon data is needed both to achieve better accuracy and to resolve a possible theoretical problem with the shape of the p_t distribution observed in existing experiments.[27] New collider data from the CDF collaboration covering a much smaller x range are becoming available and better fixed-target measurements are anticipated from the on-going analysis of the E706 experiment. In addition, a wealth of data on jet-production from CDF and D0, which are even more sensitive to gluons, are also becoming

available. This promises to be an active area of investigation to gain information on $G(x,Q)$ in hadron colliders. These efforts will complement well parallel ones actively pursued at HERA.

◦ $\mathbf{d(x,Q)/u(x,Q)}$: The d/u ratio not only directly impacts on the W-charge asymmetry (y-dependence), it also has an influence on the p_T distribution of decaying leptons in W-production which is critical to the understanding of precision measurement of the W mass. How can one assess the uncertainties on the parton distributions which affect QCD predictions on these important quantities? As mentioned earlier, using the range spanned by some set of canned distributions which fit the A_W data to varying degrees of goodness as an estimate on the uncertainty is not a satisfying strategy. In the current round of CTEQ analysis, we have performed a number of studies to explore this problem.

As an example, we show in Fig.21a two fits to the global data in addition to CTEQ3M with the requirement that the "upper" one gives rise to a W-lepton asymmetry A_W about one standard deviation above the CDF data, and the "lower" one to values of A_W one standard deviation below the CDF data. The slope of the d/u ratio from these three sets of parton distributions are shown in Fig.21b. Since all three sets give rise to comparable fits to the rest of the global data sets (with CTEQ3M being the best fit), the differences exhibited here perhaps represent more realistically the uncertainty associated with this quantity.

The W-mass measurement, although also sensitive to the d and u distributions, is not dependent on this same quantity. To arrive at a meaningful assessment of the uncertainties due to parton distributions, it is desirable to perform a similar study as above but focused on the p_t spectrum on which the mass determination depends. Such a study is underway.

◦ **SU(2) Flavor asymmetry of sea quarks** $-$ $(\bar{d}-\bar{u})$**:** As noted in the previous section, important progress has been made on the difference between $\bar{u}$ and $\bar{d}$ quarks. The main contributing processes are DIS structure functions on proton, deuterium and nuclear targets, lepton-pair production, and the recent A_W measurement. Do the differences between the MRSA and CTEQ3M $(\bar{d}-\bar{u})$ function shown in Fig.18 reflect the current uncertainty on this quantity? (This question has important bearing on the validity of the Gottfried Sum Rule.) A closer look at the $\chi^{2\prime}s$ for these two sets shown in Table 4 indicates that over half of the difference comes from the very precise BCDMS sets. A further examination of the individual data points reveals that much of the extra χ^2 occurs at the small-x end of the BCDMS D_2 data set. This is the x range where the $(\bar{d}-\bar{u})$ function shows a difference in Fig.18. This difference may be partially related to our exclusion of the conflicting CCFR and NMC F_2 data below $x = 0.09$. One theoretical uncertainty in this region concerns the size of shadowing corrections to the deuterium measurement. We have made independent analyses with and without deuterium corrections (based on Ref.[44]) and found that the differences between the resulting parton distributions were insignificant, and that the above conclusions were unaffected.

In order to obtain a self-contained estimate of the uncertainty of the $(\bar{d}-\bar{u})$ function, we have performed a series of fits systematically varying the a_1 parameter of this function at Q_0. Fig.22 shows a band of curves representing the resulting $(\bar{d}-\bar{u})$ at $Q = 5$ GeV. The overall χ^2 of these fits, as well as their distribution among the various experiments, are very similar – except that those vanishing faster toward small-x in general give better fits to the CDF A_W data. This band plot gives an indication on the uncertainty of $(\bar{d}-\bar{u})$ under the

conditions described above. A more detailed study of this problem and its implication on the Gottfried sum rule is still underway. We remark that there is a proposed (and approved) experiment at Fermilab, E866, which will measure this quantity over the kinematic region in question. With the recent developments, this measurement acquires even more significance.

◦ **SU(3) Flavor asymmetry of sea quarks – $\mathbf{s(x,Q)}$** : As discussed in some detail in Sections 4.1-4.3, the strange quark distribution is not included in current global analyses on the same footing as the non-strange quarks. The MRS and CTEQ3 analyses both adopt the assumption that $s(x,Q) = (\bar{d}+\bar{u})/4$. This is consistent with the neutrino dimuon data; but causes problems with the available inclusive $F_2^{\nu N}$ and $F_2^{\mu N}$ data at small-x. To see this problem, we show in Fig.23 the $F_2^{\nu N}$ and $F_2^{\mu N}$ data in the range $0.01 < x < 0.1$ and $Q^2 > 4$ GeV^2 compared to CTEQ3M and MRSA curves.[16] The CTEQ2 and CTEQ3 analyses leave out these data points because their simultaneous inclusion is inconsistent with the assumption made on the strange distribution in the fitting process, as revealed in the CTEQ1 analysis. The MRS analyses include these data in the fit, seeking a best comprise. Thus, the MRSA curves are closer to the data points in Fig.23, but at the expense of higher overall χ^2 – particularly on the BCDMS measurements. It appears that, this discrepancy needs to be understood before we can have complete confidence in our knowledge on $s(x,Q)$.

7 Summary and Conclusions

The sequence of analyses reported here give a realistic view of the manner in which progress in theory and experiment interact as the characteristics of the various parton distributions are investigated. The latest version of CTEQ analysis, CTEQ3, provides an excellent description of a wealth of data covering an extended range in both Q^2 and x compared to what was available just a few years ago. The precision of the data and the diversity of physical processes together allow detailed investigations of *fine structures* such as the breaking of flavor symmetry in the sea. Where possible we indicated remaining sources of uncertainty and suggested what types of data might help to reduce this in the future. One interesting area concerns the small-x behavior of the gluon and how to reconcile its behavior there with observables which are sensitive to the behavior at moderate to large values of x. Certainly future collider measurements of jet and photon production will play a leading role in such studies. The remaining uncertainties on quark distributions concern detailed flavor differentiation, particularly among the sea quarks. New measurements on vector boson production (W-, Z- and continuum lepton-pair) will be valuable, as illustrated by the first CDF results on A_w and NA51 on A_{DY}; and clarification of the difference between $F_2^{\nu N}$ and $F_2^{\mu N}$ data in the range $0.01 < x < 0.1$ is sorely needed.

Related projects which are underway and will be reported separately cover a range of topics relevant to the global analysis of PDF's. These include a comprehensive survey of direct photon measurements spanning the range from fixed target to collider energies, a detailed examination of issues related to the choice of parametrizations and the effects on

[16]The $F_2^{\nu N}$ points are converted from $F_2^{\nu Fe}$ data by using the ratio $F_2^{\mu D}/F_2^{\mu A}$, (A = Ca, Fe), measured by NMC. The NMC ratio is consistent with the only, much less accurate, neutrino shadowing measurement [45], and with predictions from PCAC [46].

the description of individual experiments, and a method of estimating errors on predictions due to the uncertainties associated with the parton distribution determinations.

The results presented here should be considered in the same sense as a snapshot showing the state of the subject at one instant of time. As new data and calculations become available, the underlying QCD framework will be ever more critically tested, and further progress toward a unique determination of parton distributions will be made.

Acknowledgement

We would like to thank our colleagues in the CTEQ Collaboration for many lively discussions and useful suggestions. We also would like to note that a global analysis project of this scope necessarily involves indirect contributions from a wide spectrum of sources worldwide through constant communications with many physicists, particularly some key members of experiments whose data are used in the analyses. These sources are too numerous to name individually. Likewise, the programs used to perform these analyses, although mostly developed by us, do contain elements from other sources and involve some contribution from our CTEQ colleagues, to all of whom we express our thanks.

References

[1] For a review and detailed references, see J.F. Owens and W.K. Tung, "Parton Distributions of Hadrons" in *Ann. Rev. Nucl. Sci.*, **42**, 291 (1992).

[2] Wu-Ki Tung, *Proceedings of International Workshop on Deep Inelastic Scattering and Related Subjects*, Eilat, Israel, 1994 World Sci., Singapore (to be published).

[3] D. Duke and J. Owens, *Phys. Rev.* **D30**, 49 (1984).

[4] A. Devoto, D.W. Duke, J.F. Owens, and R.G. Roberts, *Phys. Rev.* **D27**, 508 (1983).

[5] J.G. Morfin and W.K. Tung, *Z. Phys.* **C52** 13, (1991).

[6] J. Botts, J.G. Morfin, J.F. Owens, Jianwei Qiu, Wu-Ki Tung, and H. Weerts, *Phys. Lett.* **B304**, 159 (1993).

[7] CCFR Collaboration (W.C. Leung, et al.), *Phys. Lett.* **B317**, 655 (1993); and (P.Z. Quintas, et al.), *Phys. Rev. Lett.* **71**, 1307 (1993).

[8] NMC Collaboration (P. Amaudruz, et al.), *Phys. Lett.* **B295**, 159 (1992).

[9] ZEUS Collaboratio, *Phys. Lett.* **B316**, 412 (1993); H1 Collaboration, *Nucl. Phys.* **B407**, 515 (1993).

[10] CDF Collaboration, Preprint FERMILAB-CONF-94/146-E. (1994).

[11] NA51 Collaboration (A. Baldit, et al.), *Phys. Lett.* **B332**, 244 (1994).

[12] A.D. Martin, W.J. Stirling, and R.G. Roberts, *Phys. Rev.* **D47**, 867 (1993); *Phys. Lett.* **B306**, 145 (1993).

[13] A.D. Martin, W.J. Stirling, and R.G. Roberts, RAL-94-055 and DTP/94/93.

[14] D.W. Duke, J.F. Owens, and R.G. Roberts, *Nucl. Phys.* **B195**, 285 (1982).

[15] BCDMS Collaboration (A.C. Benvenuti, *et.al.*.), *Phys.Lett.*, **B223,** 485, (1989); and *Phys. Lett.,***B237,** 592, (1990).

[16] L.W. Whitlow et al., *Phys. Lett.* **B282**, 475 (1992); and (A. Bodek et al.), *Phys. Rev.* **D20**, 1471 (1979).

[17] J.J. Aubert *et.al.*, *Nucl. Phys.* **B293**, 740 (1987); K. Bazizi, S.J. Wimpenny, and T. Sloan, *Proceedings of the 25th International Conference on High Energy Physics*, Singapore, (1990).

[18] H. Abramowicz, *et al.*, *Phys. Rev. Lett.*, **57**, 298 (1986); *Z. Phys.* **C28**, 51 (1985); J.P. Berge, *et al.*, *Z. Phys.* **C49**, 187 (1991).

[19] J. Gomez et al., *Phys. Rev.* **D49**, 4348 (1994); R.G. Arnold et al., *Phys. Rev. Lett.* **52**, 727 (1984).

[20] EMC Collaboration: Arneodo, M. et.al., *Nucl. Phys.* **B331**:1 (1990); J. Ashman, *et al., Z. Phys.*, **C57**, 211 (1993).

[21] NMC Collaboration (R. Seitz and A. Witzmann) in *Proceedings of the XXVIIIth Rencontre de Moriond*, Ed. Tran Thanh Van, Editions Frontieres, (1993)

[22] E605: (G. Moreno, *et al.*, *Phys. Rev.*, **D43**, 2815 (1991).

[23] CDF Collaboration, *Phys. Rev.* **D49**, R1 (1994).

[24] M. Bonesini *et al.*, *Z. Phys.* **C38**, 371 (1988).

[25] A. Bernasconi *et al.* (UA6 Collaboration). *Phys. Lett.* **B206**, 163 (1988).

[26] G. Alverson *et al.* (E706 Collaboration). *Phys. Rev.* **D48**, 5 (1993).

[27] J. Huston et al. (to be published) Preprint MSU-HEP/41027.

[28] S.D. Ellis and W.J. Stirling, *Phys. Lett.* B256, 258 (1991).

[29] NMC Collaboration (M. Arneodo, et al.), *Phys. Rev.* **D50**, 1 (1994).

[30] J.C. Collins and Wu-Ki Tung, *Nucl. Phys.* **B278**, 934 (1986).

[31] M.G. Aivazis, J.C. Collins, F. Olness & Wu-Ki Tung, *Phys. Rev.* **D50**, 3102 (1994).

[32] CCFR Collaboration A. Bazarko in Proceedings of 18th Rencontres de Moriond, Ed. Tran Thanh Van, Editions Frontieres, (1993).

[33] CDHSW Collaboration (H. Abramowicz *et al.*), *Phys. Rev. Lett.* **57**, 298 (1986); *Z. Phys.*, **C28**, 51 (1985).

[34] Charm Collaboration (J.V. Allaby, *et al.*), *Z. Phys.* **C36**, 611 (1987); *Phys. Lett.* **197B**, 281 (1987); *Phys. Lett.* **B213**, 554 (1988).

[35] CCFR Collaboration (K. Lang *et.al.*), *Z. Phys.* **C33**, 483 (1987); Rabinowitz*et al., Phys. Rev. Lett.*, **70** 134 (1993).

[36] M.G. Aivazis, F. Olness & Wu-Ki Tung, *Phys. Rev. Lett.* **65**, 2339 (1990).

[37] M. Shaevitz in *Results and Perspectives in Particle Physics*, La Thuile, 1993.

[38] R. Voss, in *Proceedings of XVI International Symposium on Lepton and Photon Interactions*, Ithaca , NY, Ed. P. Drell and D. Rubin, Pub. AIP (1994).

[39] U. Baur, F. Halzen, S. Keller, M.L. Mangano, and K. Riesselmann, *Phys. Lett.* **B318**, 544 (1993).

[40] S. Keller, W.T. Giele, and E. Laenen, Fermilab-Conf-94/260-T (to be published in the Proceedings of DPF'94).

[41] ZEUS Collaboration M. Lancaster, Invited talk given at the 27th International Conference on High Energy Physics, July 1994, Glasgow Scotland.

[42] S. Bethke, *42nd Scottish Universities Summer School in Physics (SUSSP 93): High Energy Phenomenology (NATO Advanced Study Institute)*, St. Andrews, Scotland, Aug 1993 Heidelberg preprint HD-PY-93-07.

[43] T. Jaroscewicz, *Phys. Lett.*‘ **116B**, 291 (1982).

[44] W. Melnitchouk and A.W. Thomas, *Phys. Rev.* **D47**, 3783 (1993); B. Badelek and J. Kwiecinski, *Nucl. Phys.* **B370**, 278 (1992).

[45] BEBC WA59 Collaboration (P.P. Allport, et al.), *Phys. Lett.* **B232**, 417 (1989).

[46] J.S. Bell, *Phys. Rev. Lett.* **13**, 57 (1964).

Figure Captions

Figure 1 A comparison of the data for A_{DY} from NA51 with NLO QCD results obtained from previous and current versions of MRS and CTEQ parton distributions.

Figure 2 The CDF W lepton charge asymmetry data compared to NLO QCD results obtained from previous and current versions of MRS and CTEQ parton distributions.

Figure 3 Comparison of the current ZEUS small-x data at $Q^2 = 15$ GeV^2 with various parton distribution sets with different x exponent values.

Figure 4 Comparison of the CTEQ3 fit with $F_2^{\mu N}$ data of BCDMS and NMC experiments. The absolute vertical scale is not labelled since an offset factor has been applied to the various x bins to avoid overlap.

Figure 5 Comparison of the CTEQ3 fit with $F_2^{\mu n}/F_2^{\mu p}$ data of the NMC experiment.

Figure 6 Comparison of the CTEQ3 fit with $F_2^{\nu N}$ data of the CCFR experiment. Data points are converted from the measured $F_2^{\nu Fe}$ by using the ratio $F_2^{\mu D}/F_2^{\mu Fe}$ measured by NMC.

Figure 7 Comparison of the CTEQ3 fit with $F_3^{\nu N}$ data of the CCFR experiment. Data points are converted from the measured $F_3^{\nu Fe}$ as for $F_2^{\nu N}$.

Figure 8 Comparison of the CTEQ3 fit with current $F_2^{\mu p}$ data of the ZEUS experiment.

Figure 9 Comparison of the CTEQ3 fit with the double differential cross-section data of the E606 lepton-pair production (Drell-Yan) experiment.

Figure 10 Comparison of the CTEQ3 fit with $d\sigma/dp_t$ data of three fixed target direct photon production experiments.

Figure 11 An overview of all parton distribution functions at $Q = 5$ GeV from the new CTEQ3M analysis.

Figure 12 Comparison of the valence u quark distribution at $Q = 5$ GeV from the current and previous versions of CTEQ and MRS sets.

Figure 13 Comparison of the valence d quark distribution at $Q = 5$ GeV from the current and previous versions of CTEQ and MRS sets.

Figure 14 Comparison of the gluon distribution at $Q = 5$ GeV from the current and previous versions of CTEQ and MRS sets.

Figure 15 Comparison of the sea quark distribution $\bar{u}$ at $Q = 5$ GeV from the current and previous versions of CTEQ and MRS sets.

Figure 16 Comparison of the sea quark distribution $\bar{d}$ at $Q = 5$ GeV from the current and previous versions of CTEQ and MRS sets

Figure 17 Comparison of the strange quark distribution at $Q = 5$ GeV from the current and previous versions of CTEQ and MRS sets

Figure 18 A comparison of the results for the $\overline{d} - \overline{u}$ difference from various sets of distributions.

Figure 19 A comparison of the results for the ratio d/u from various sets of distributions.

Figure 20 The gluon distribution at $Q = 5$ GeV in the ranges – (a) $0.1 < x < 0.6$, and (b) $10^{-4} < x < 0.6$ – from CTEQ3M, MRSA and from the alternative CTEQ2 sets which are designed to explore various aspects of parton distribution uncertainties.

Figure 21 (a) Three fits bracketing the CDF W lepton-asymmetry data; (b) The corresponding slopes of the d/u ratio of the three sets of parton distributions.

Figure 22 A band of $(\bar{d} - \bar{u})$ from a series of global fits which yield comparable χ^2's.

Figure 23 Comparison of (a) CCFR neutrino and (b) NMC muon measurements of F_2 in the $0.015 < x < 0.09$ region compared to MRSA and CTEQ3M curves. These data points are excluded from the CTEQ2 and CTEQ3 fits since, taken together, they conflict with the strange quark distribution adopted in the fit.

Process	Experiment	Observable	Data Points	$\Delta\sigma$	Set
DIS	BCDMS	$F_{2\ H}^{\mu}$	168	.02	1
		$F_{2\ D}^{\mu}$	156	.02	1
	NMC	$F_{2\ H}^{\mu}$	52	.02	1
		$F_{2\ D}^{\mu}$	52	.02	1
	H1	$F_{2\ H}^{\mu}$	21	.04	2
	ZEUS	$F_{2\ H}^{\mu}$	56	.03	2
	CCFR	$F_{2\ Fe}^{\nu}$	63	.02	1
		$x\ F_{3\ Fe}^{\nu}$	63	.02	1
	NMC	F_2^n/F_2^p	89	-	1
Drell-Yan	E605	$sd\sigma/d\sqrt{\tau}dy$	119	.1	1
	CDF	$sd\sigma/d\sqrt{\tau}dy$	8	.1	2
	NA-51	A_{DY}	1	-	3
W-prod.	CDF	Lepton asym.	9	-	3
Direct γ	WA70	$Ed^3\sigma/d^3p$ $1.0 \geq y \geq -.75$	39	.10	1
	E706	$Ed^3\sigma/d^3p$ $y = 0$	8	.15	1
	UA6	$Ed^3\sigma/d^3p$ $y = .3$	16	.10	1

Table 1: The data sets used in the CTEQ global analyses. Data sets marked with 1 in the final column were used for the CTEQ1 and later fits. Those with a 2 or 3 were added for the CTEQ2 and CTEQ3 analyses respectively. The column labelled $\Delta\sigma$ gives the overall normalization systematic error used in defining the χ^2, as discussed in the text.

Distribution	Parameter	2M	2MS	2MF	2ML	2D	2L
xu_v	a_0^u	.269	.268	.261	.266	.307	.164
	a_1^u	.278	.276	.276	.289	.254	.175
	a_2^u	3.67	3.66	3.66	3.58	3.44	3.32
	a_3^u	29.6	29.1	29.8	30.2	25.5	44.1
	a_4^u	.807	.801	.795	.799	.917	.961
xd_v	a_0^d	1.24	1.32	1.18	1.46	1.17	1.08
	a_1^d	.521	.538	.508	.565	.511	.493
	a_2^d	3.18	3.26	3.24	3.46	3.16	3.00
	a_3^d	-0.85	-0.84	-0.83	-0.59	-0.60	-1.00
	a_4^d	1.82	1.85	2.19	2.32	2.31	2.99
xg	a_0^g	.900	.197	3.05	.825	.711	.521
	a_1^g	-.258	-.500	.000	-.212	-.240	-.259
	a_2^g	5.19	3.82	6.53	4.55	4.84	4.61
	a_3^g	5.13	5.81	2.64	12.0	7.43	16.3
	a_4^g	1.12	.450	2.22	1.62	.960	1.24
$x(\overline{d}+\overline{u})/2$	a_0^+	.0825	.0130	.2540	.1139	.0947	.1127
	a_1^+	-.258	-.500	.000	-.212	-.240	-.259
	a_2^+	8.45	7.62	9.40	9.14	8.76	8.94
	a_3^+	12.7	38.4	13.5	15.2	14.6	17.5
	a_4^+	1.10	0.82	1.60	1.36	1.39	1.58
$x(\overline{d}-\overline{u})$	a_0^-	.111	.105	.114	.117	.121	.103
	a_1^-	.012	.043	.085	.031	.106	.043
	a_2^-	9.53	10.00	9.71	9.95	9.00	9.87
	a_3^-	-14.8	-15.5	-15.7	-15.4	-15.7	-17.7
	a_4^-	49.4	53.8	55.7	51.7	48.2	52.3
xs	a_0^s	.156	.152	.110	.155	.140	.165
	a_1^s	-0.004	0.004	-0.128	0.001	-0.004	-0.001
	a_2^s	6.87	6.85	6.88	6.90	6.90	6.90
	$\Lambda^5(MeV)$	139	135	135	220	155	143

Table 2: CTEQ2 input parton distribution function parameters (at $Q_0 = 1.6$ GeV). The functional form used in CTEQ2 is $xf = a_0^f x^{a_1^f}(1-x)^{a_2^f}(1+a_3^f x^{a_4^f})$, where $f = u_v, d_v, gluon, (\overline{d}+\overline{u})/2$, s; and $x(\overline{d}-\overline{u}) = a_0^- x^{a_1^-}(1-x)^{a_2^-}(1+a_3^-\sqrt{x}+a_4^- x)$.

Distribution	Parameter	CTEQ3M	CTEQ3D	CTEQ3L
xu_v	a_0^u	1.37	1.36	1.29
	a_1^u	.497	.470	.452
	a_2^u	3.74	3.51	3.51
	a_3^u	6.25	6.19	6.85
	a_4^u	.880	1.04	1.11
xd_v	a_0^d	.801	.837	.858
	a_1^d	.497	.470	.452
	a_2^d	4.19	4.22	4.20
	a_3^d	1.69	2.58	2.54
	a_4^d	.375	.748	.947
xg	a_0^g	.738	.595	.404
	a_1^g	-.286	-.332	-.349
	a_2^g	5.31	5.45	5.59
	a_3^g	7.30	11.0	18.1
$x(\overline{d}+\overline{u})/2$	a_0^+	.0547	.0330	.0451
	a_1^+	-.286	-.332	-.349
	a_2^+	8.34	8.16	7.36
	a_3^+	17.5	23.2	14.5
$x(\overline{d}-\overline{u})$	a_0^-	.0795	.0702	.0566
	a_1^-	.497	.470	.452
	a_2^-	8.34	8.16	7.36
	a_3^-	30.0	27.1	29.9
xs	κ	.5	.5	.5
	$\Lambda^5(MeV)$	158	164	132

Table 3: CTEQ3 input parton distribution function parameters (at $Q_0 = 1.6$ GeV). The functional forms are described in Sec.3.3. The number of independant parton shape parameters is 15.

expt.	# of pts	CTEQ3M	MRS A	CTEQ2M	MRS D-'
$BCDMS^H$	168	130.0(0.77)	168.0(1.00)	110.2(0.66)	133.2(0.79)
$BCDMS^D$	156	187.2(1.20)	215.3(1.38)	174.7(1.12)	162.2(1.04)
NMC^H	52	59.9(1.15)	60.2(1.15)	61.5(1.18)	59.2(1.14)
NMC^D	52	47.2(0.91)	56.0(1.08)	49.1(0.94)	49.7(0.96)
NMC_R	89	133.5(1.50)	140.6(1.58)	139.7(1.57)	144.2(1.62)
CCFR F_2	63	69.3(1.10)	68.7(1.09)	58.8(0.93)	95.8(1.52)
CCFR F_3	63	41.0(0.65)	61.7(0.98)	37.2(0.59)	67.4(1.07)
ZEUS	56	27.9(0.50)	40.3(0.72)	27.9(0.50)	74.5(1.33)
H1	21	7.7(0.37)	7.0(0.33)	6.4(0.30)	11.7(0.56)
E605	119	92.3(0.78)	95.9(0.81)	88.1(0.74)	102.6(0.86)
CDF DY	8	3.0(0.38)	1.4(0.18)	2.6(0.32)	2.8(0.34)
CDF A_W	9	3.5(0.39)	3.4(0.38)	12.2(1.36)	3.8(0.42)
NA51 A_{DY}	1	0.4(0.35)	0.0(0.03)	3.0(3.02)	10.3(10.3)
WA70	39	23.3(0.60)	21.3(0.55)	22.6(0.58)	21.4(0.55)
E706	8	11.8(1.47)	11.2(1.40)	12.2(1.52)	11.3(1.41)
$UA6^{\bar{P}P}$	8	1.8(0.23)	1.6(0.20)	2.2(0.27)	1.5(0.19)
$UA6^{PP}$	8	6.8(0.85)	6.8(0.85)	7.5(0.94)	6.8(0.85)
Total	920	844	959	816	958

Table 4: χ^2 and χ^2 per point (in paranthesis) in each experiment and overall for current and previous version of CTEQ and MRS distributions. In the case of the MRS distributions, we have *minimized* the χ^2 by adjusting all the experimental normalizations *freely* while keeping the parton distributions as given by the authors. (See Table 5.) These χ^2 values are obtained using the data sets of Table 1, employing the same error definitions (except for experimental normalization for which the CTEQ numbers include extra χ^2's for any deviation away from unity as explained in the text); hence they are not necessarily the same as those quoted in the original work which may use a different selection of data points (e.g. for Drell-Yan, and direct photon experiments), apply different error definitions, and adopt different analysis procedures. Large differences in the total χ^2 are mainly associated with the precise BCDMS and CCFR experiments. They may be partially attributed to the influence on the fits due to the $x < 0.09$ data points of CCFR and NMC which are excluded in the CTEQ analyses for consistency considerations, but included in the MRS ones.

expt.	CTEQ3M	MRS A	CTEQ2M	MRS D-'
BCDMS	0.988	0.977	0.988	0.969
NMC_{90}	1.008	1.008	1.009	0.996
NMC_{280}	1.021	1.014	1.021	1.000
CCFR	0.975	0.968	0.979	0.958
ZEUS	0.978	1.029	1.003	1.061
H1	0.966	0.978	0.956	1.043
E605	1.098	1.008	1.063	1.052
CDF DY	0.965	0.805	0.971	0.970
WA70	1.010	1.055	1.023	0.977
E706	0.923	0.980	0.960	0.912
$UA6^{\bar{P}P}$	0.858	0.853	0.878	0.813
$UA6^{PP}$	0.853	0.900	0.892	0.834

Table 5: Normalization factors for experiments obtain in the CTEQ fits according to error treatment procedure described in the text. For comparison, also listed are normalization factors obtained by fitting the same data sets using the (fixed) MRS distributions and allowing all the experimental normalizations to adjust *freely*.

Fig. 1

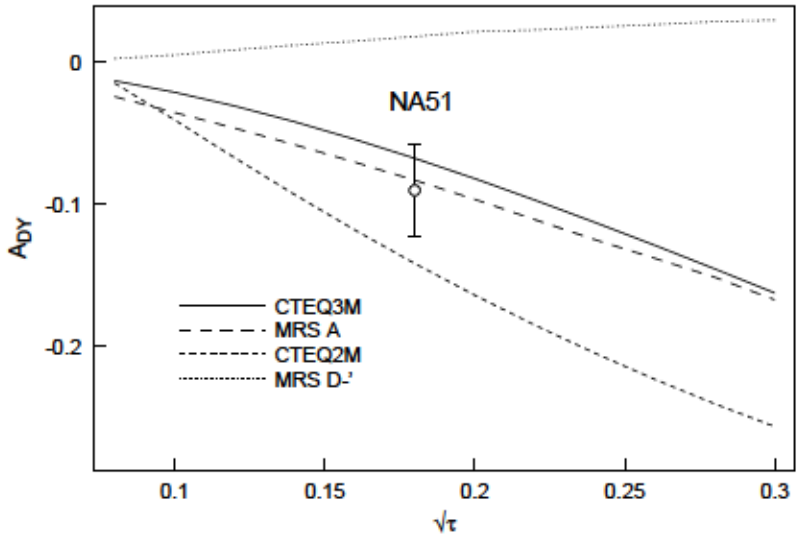

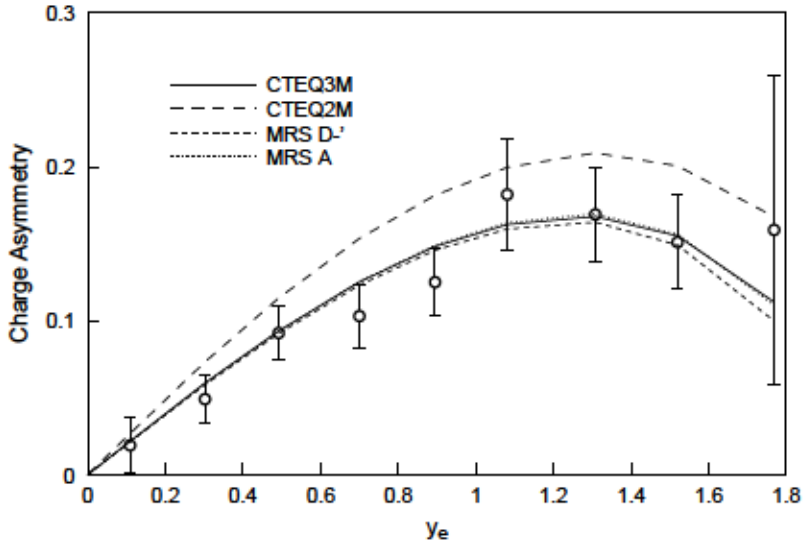

Fig. 2

Fig. 3

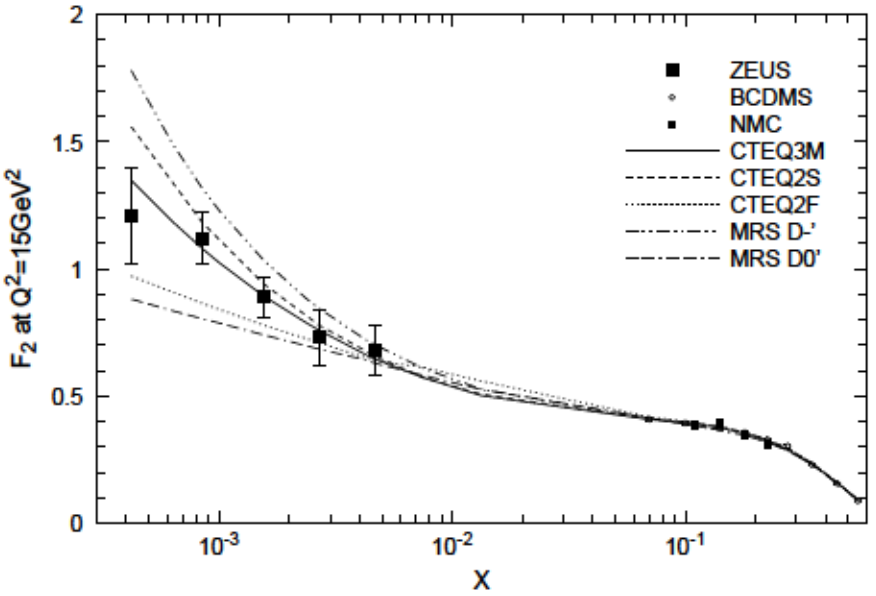

Fig. 4

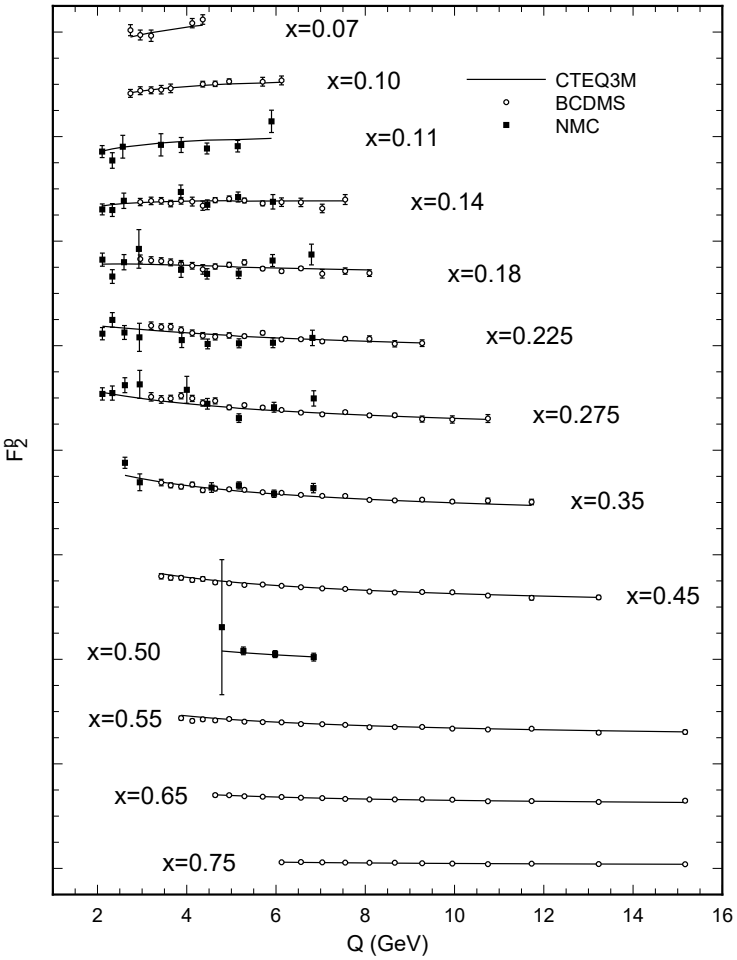
x=0.07
x=0.10
x=0.11
x=0.14
x=0.18
x=0.225
x=0.275
x=0.35
x=0.45
x=0.50
x=0.55
x=0.65
x=0.75
CTEQ3M
BCDMS
NMC
F_2^p
Q (GeV)
2
4
6
8
10
12
14
16

Fig. 5

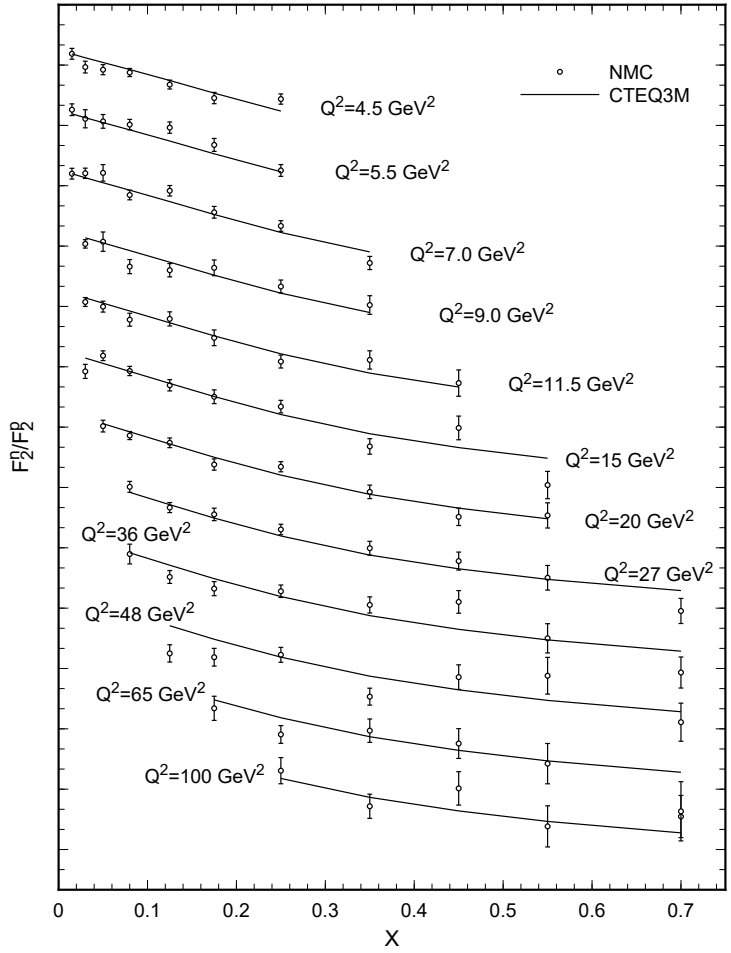
NMC
CTEQ3M
Q^2=4.5 GeV^2
Q^2=5.5 GeV^2
Q^2=7.0 GeV^2
Q^2=9.0 GeV^2
Q^2=11.5 GeV^2
Q^2=15 GeV^2
Q^2=20 GeV^2
Q^2=27 GeV^2
Q^2=36 GeV^2
Q^2=48 GeV^2
Q^2=65 GeV^2
Q^2=100 GeV^2
F_2^n/F_2^p
X
0
0.1
0.2
0.3
0.4
0.5
0.6
0.7

Fig. 6

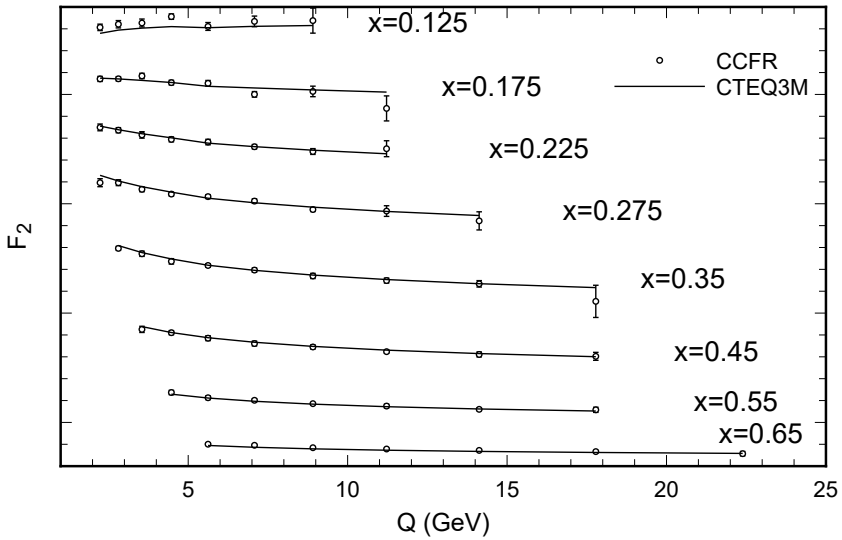

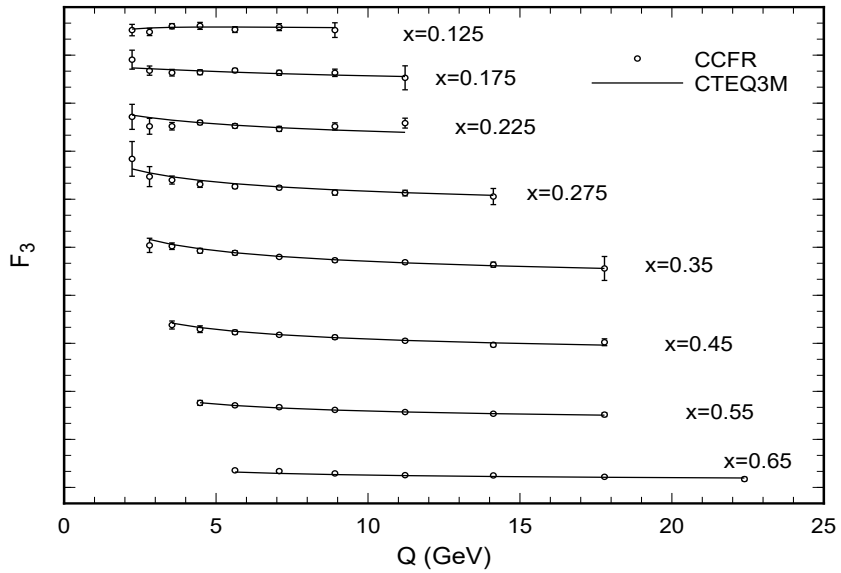

Fig. 7

Fig. 8

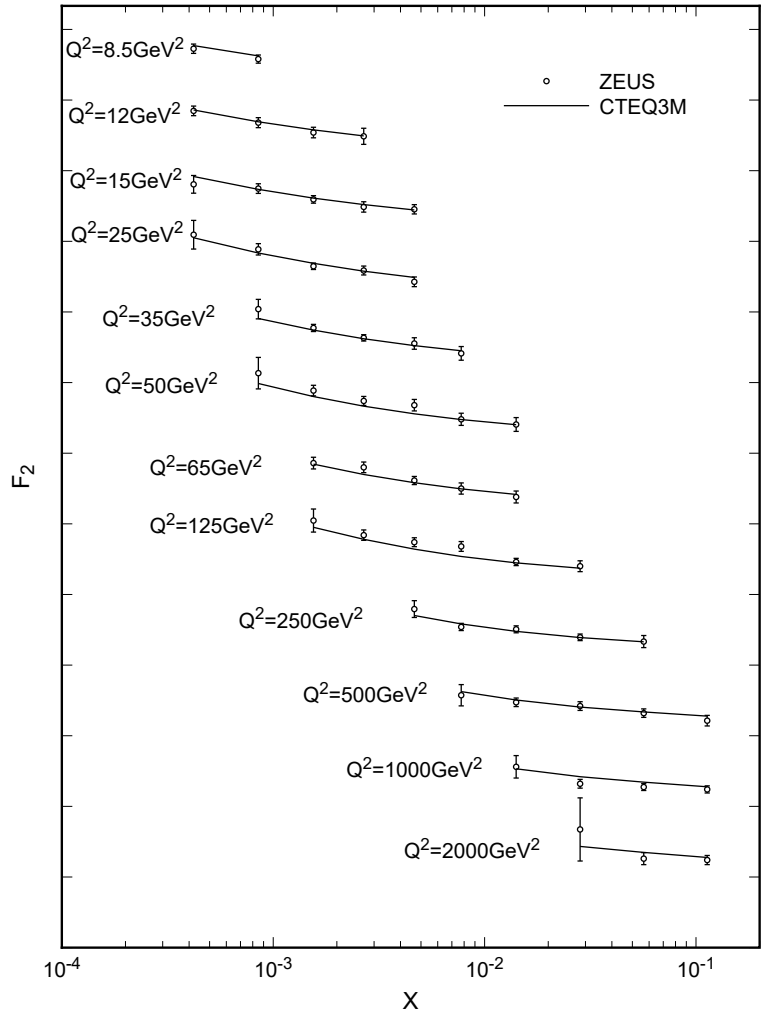

Fig. 9

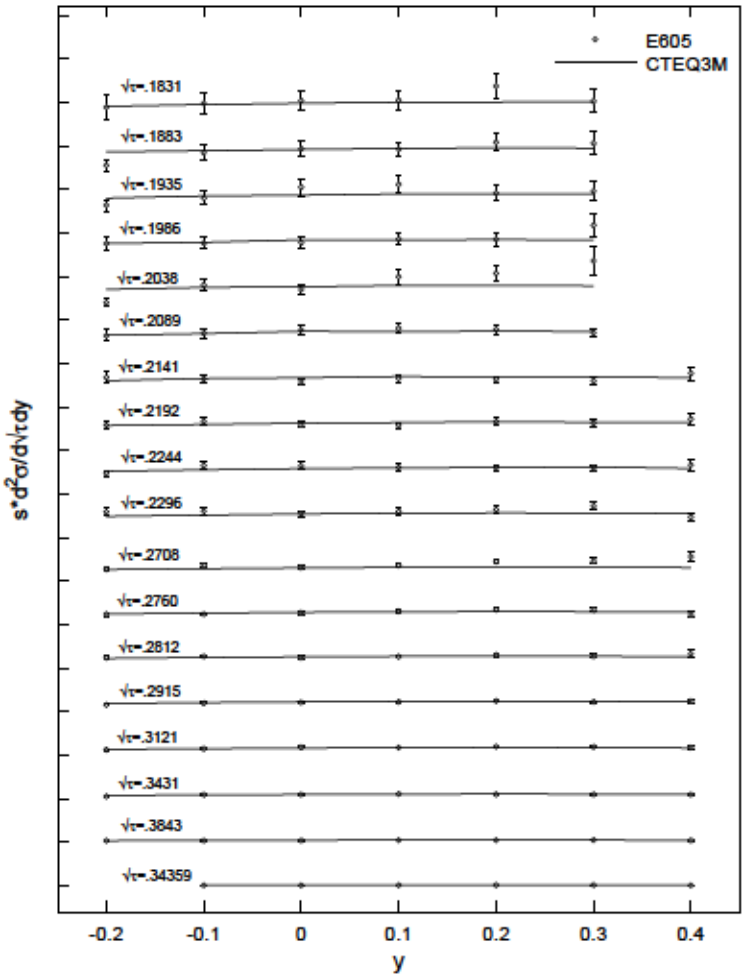

Fig. 10

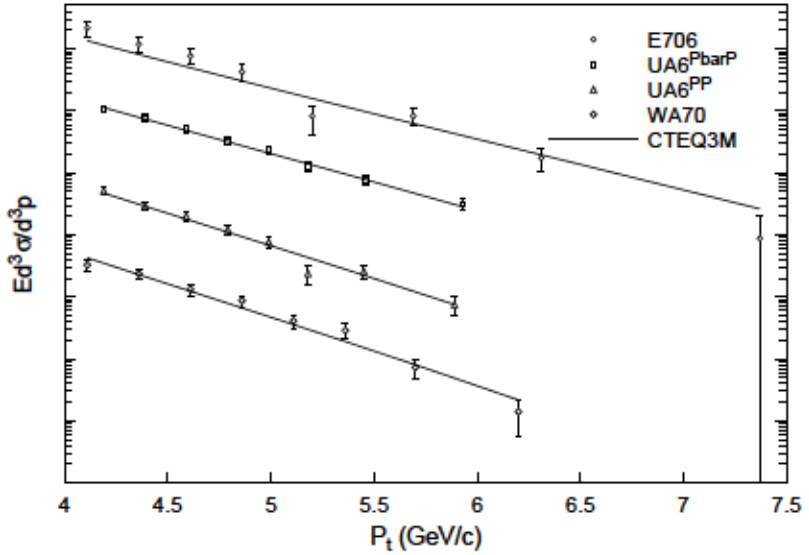

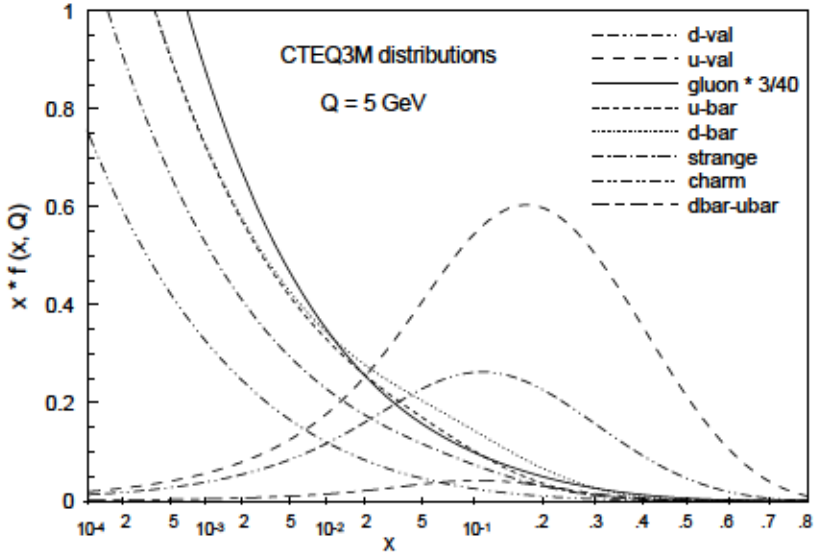

Fig. 11

Fig. 12

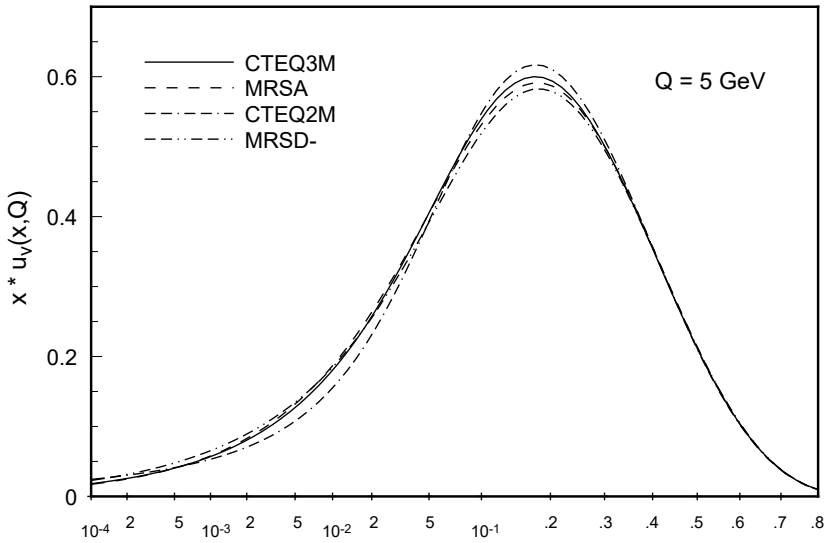

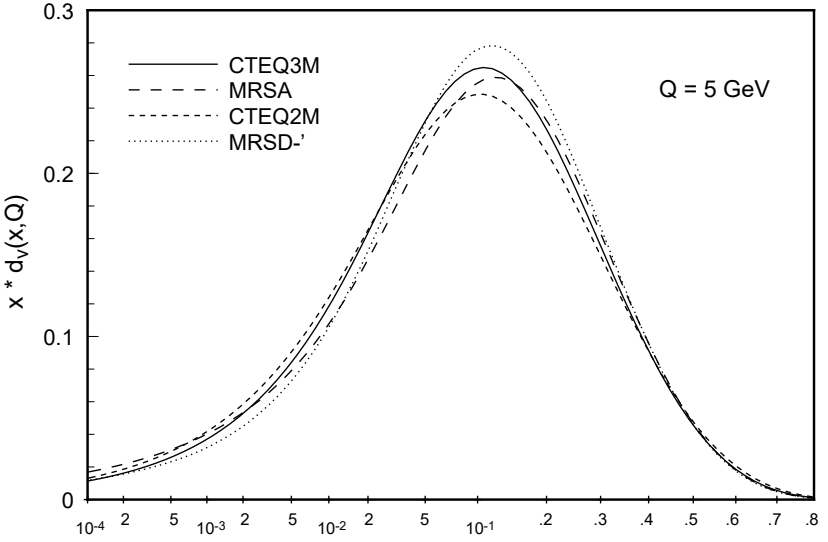

Fig. 13

Fig. 14

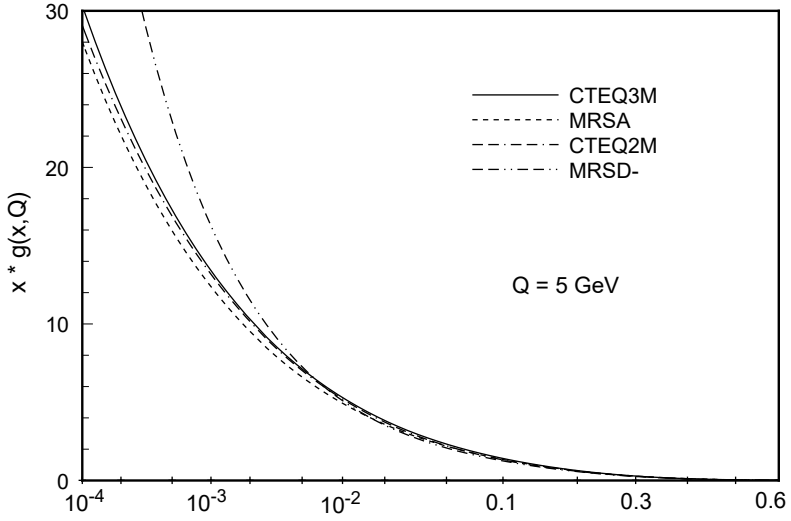

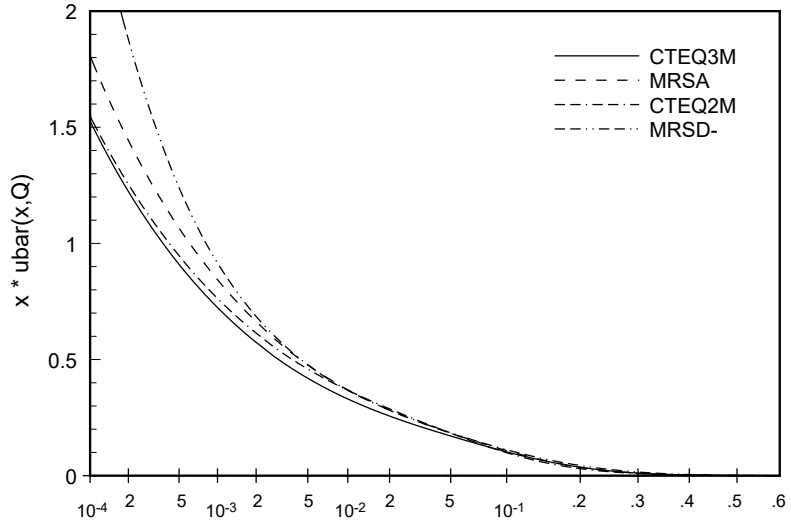

Fig. 15

Fig. 16

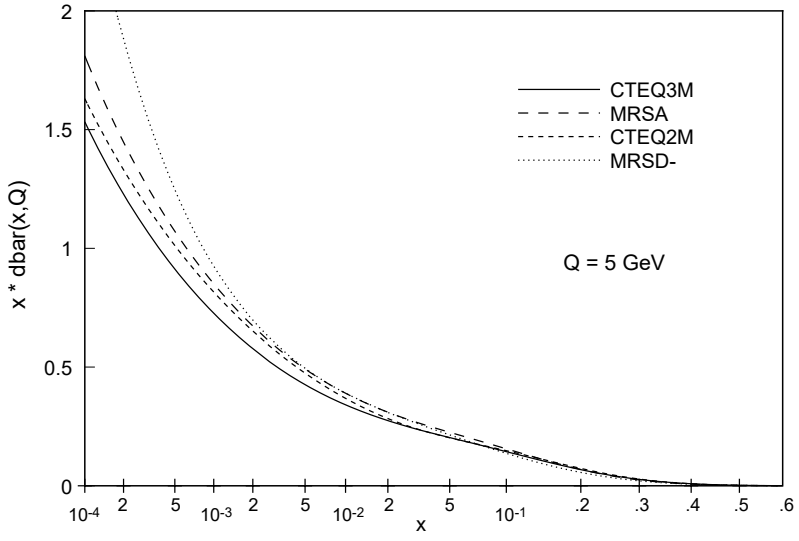

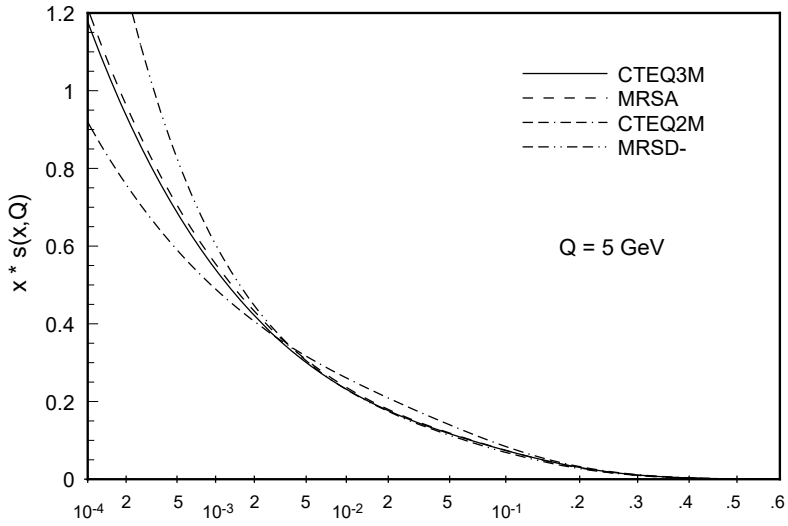

Fig. 17

Fig. 18

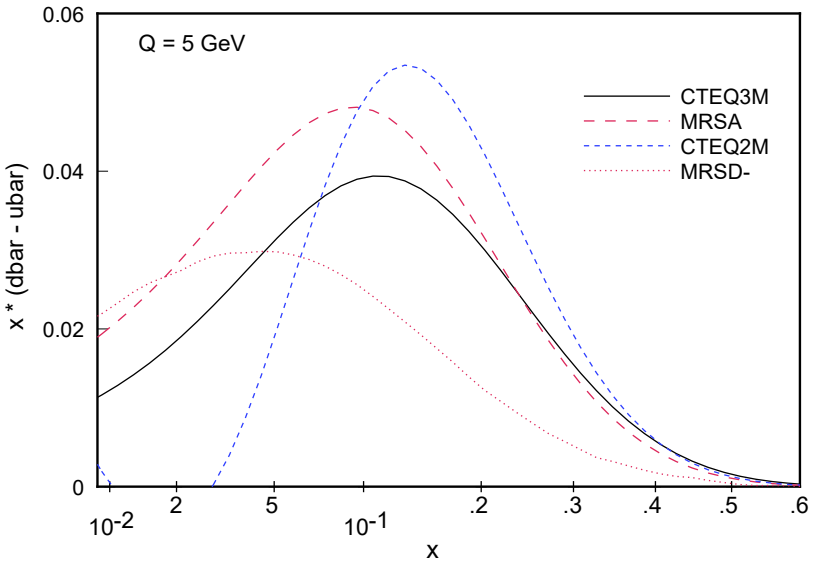

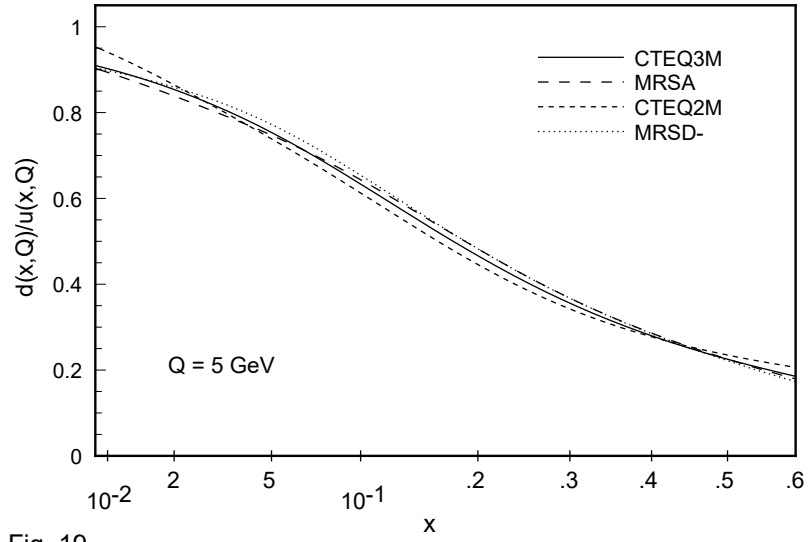

Fig. 19

Fig. 20a

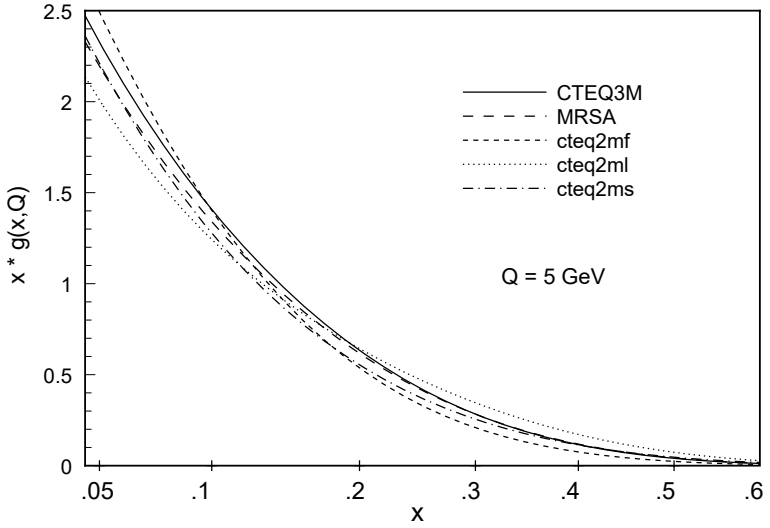

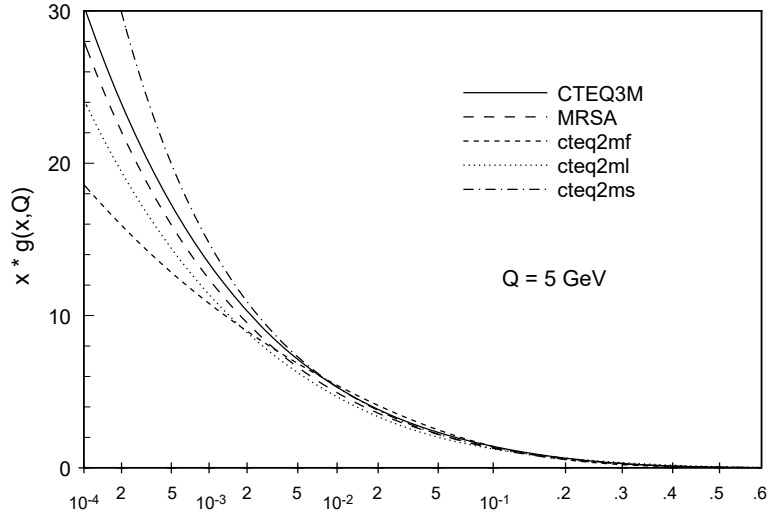

Fig. 20b

Fig. 21a

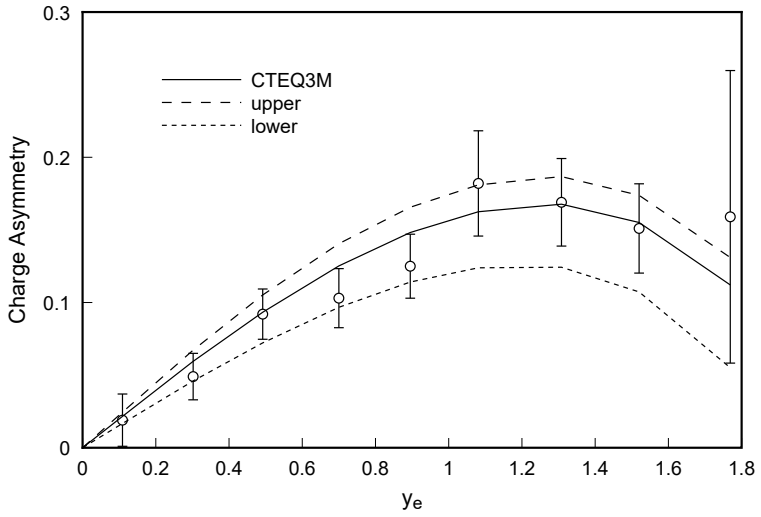

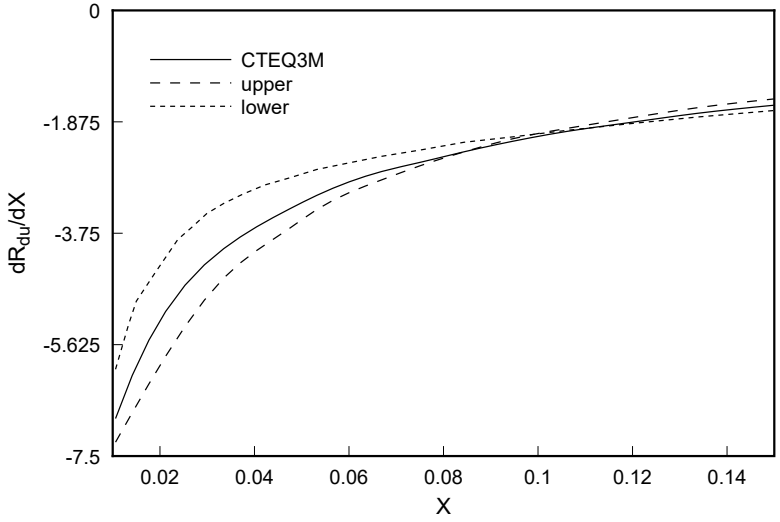

Fig. 21b

Fig. 22

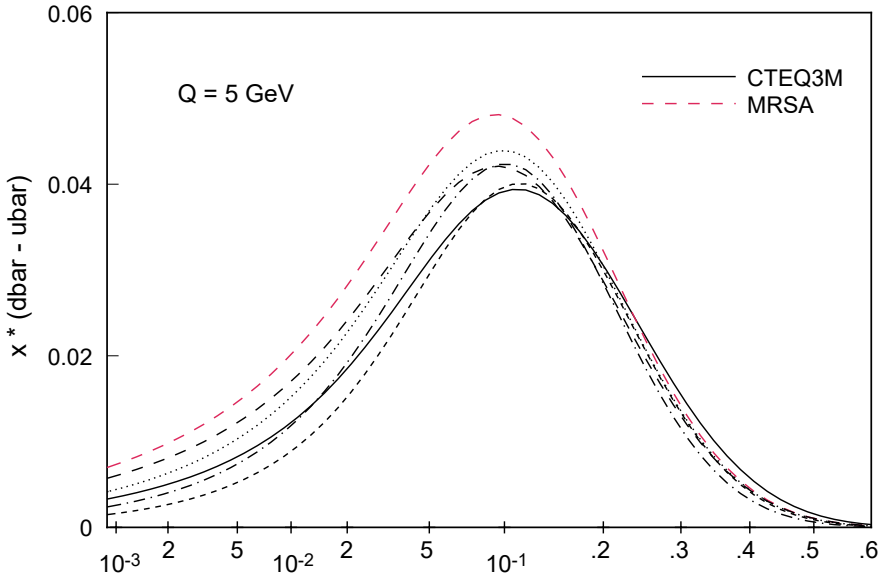
0.06
0.04
0.02
0
x * (dbar - ubar)
Q = 5 GeV
CTEQ3M
MRSA
10-3
2
5
10-2
2
5
10-1
.2
.3
.4
.5
.6

Fig. 23

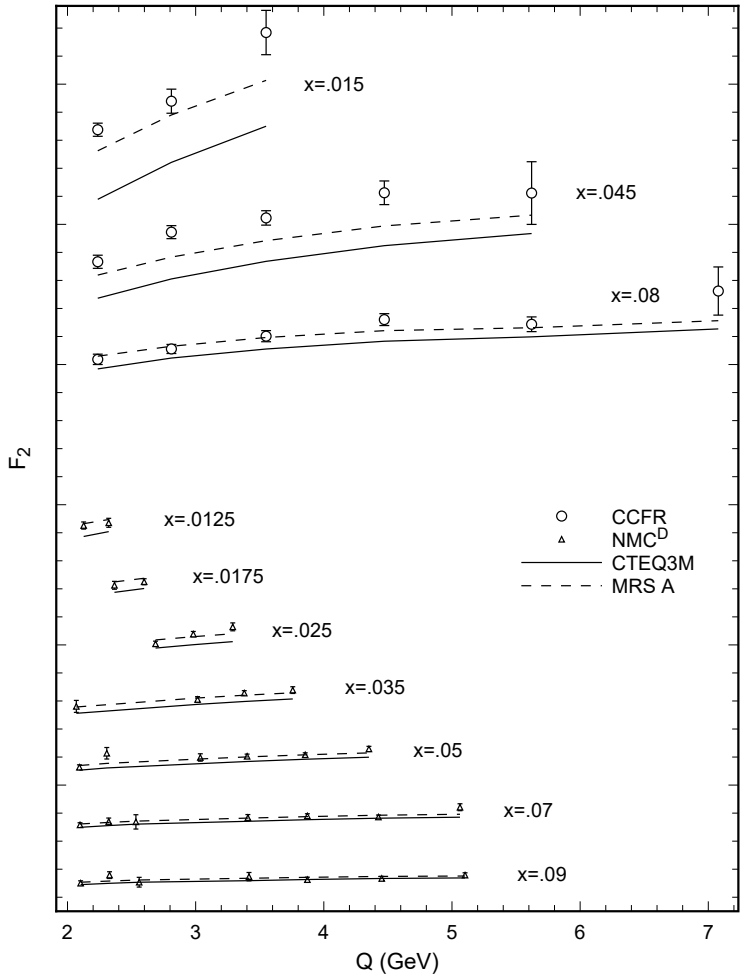
F2
x=.015
x=.045
x=.08
x=.0125
x=.0175
x=.025
x=.035
x=.05
x=.07
x=.09
CCFR
NMCD
CTEQ3M
MRS A
2
3
4
5
6
7
Q (GeV)

This figure "fig1-1.png" is available in "png" format from:

http://arxiv.org/ps/hep-ph/9410404v3

This figure "fig1-2.png" is available in "png" format from:

http://arxiv.org/ps/hep-ph/9410404v3

This figure "fig1-3.png" is available in "png" format from:

http://arxiv.org/ps/hep-ph/9410404v3

This figure "fig1-4.png" is available in "png" format from:

http://arxiv.org/ps/hep-ph/9410404v3

This figure "fig1-5.png" is available in "png" format from:

http://arxiv.org/ps/hep-ph/9410404v3

This figure "fig1-6.png" is available in "png" format from:

http://arxiv.org/ps/hep-ph/9410404v3

This figure "fig1-7.png" is available in "png" format from:

http://arxiv.org/ps/hep-ph/9410404v3

This figure "fig1-8.png" is available in "png" format from:

http://arxiv.org/ps/hep-ph/9410404v3